CHEMISORPTION OF AROMATIC COMPOUNDS ON WELL-DEFINED PALLADIUM SURFACES: STUDIES BY ELECTRON SPECTROSCOPY AND ELECTROCHEMISTRY

A Dissertation

by

DING LI

Submitted to the Office of Graduate Studies of
Texas A&M University
in partial fulfillment of the requirements for the degree of

DOCTOR OF PHILOSOPHY

August 2010

Major Subject: Chemistry

CHEMISORPTION OF AROMATIC COMPOUNDS ON WELL-DEFINED PALLADIUM SURFACES: STUDIES BY ELECTRON SPECTROSCOPY AND ELECTROCHEMISTRY

A Dissertation

by

DING LI

Submitted to the Office of Graduate Studies of
Texas A&M University
in partial fulfillment of the requirements for the degree of

DOCTOR OF PHILOSOPHY

Approved by:

Chair of Committee,	Manuel P. Soriaga
Committee Members,	Debjyoti Banerjee
	Yi-Qin Gao
	David H. Russell
Head of Department,	David H. Russell

August 2010

Major Subject: Chemistry

ABSTRACT

Chemisorption of Aromatic Compounds on Well-Defined Palladium Surfaces: Studies by Electron Spectroscopy and Electrochemistry. (August 2010)

Ding Li, B.S., Peking University

Chair of Advisory Committee: Dr. Manuel P. Soriaga

The chemisorption of aromatic compounds, derivatized with different functional groups, on well-defined Pd(111) surfaces was studied by a combination of Auger electron spectroscopy (AES), low energy electron diffraction (LEED), high resolution electron energy loss spectroscopy (HREELS), and electrochemistry (EC).

The results of this work led to the following trends and conclusions: (a) At low concentrations, 2,5-dihydroxythiophenol (DHT) chemisorbs on a Pd surface through both diphenolic ring and thiol group. At high concentrations, it chemisorbs only through the thiol group. (b) There is extensive intermolecular attraction between the co-adsorbed thiolated quinone and thiolated hydroquinone molecules. The interaction occurs through the Pd substrate and not through space. (c) The chemisorption properties of N-heteroaromatic compounds are pH-dependent. When the nitrogen heteroatom is protonated, it becomes very weakly surface-active. When the nitrogen heteroatom is deprotonated, surface activity stronger than the diphenolic ring is exhibited. (d) On a palladium surface, the binding strengths of ligands increase in the order: phenyl ring < quinonoid ring, < N-heteroatom < I < -SH.

DEDICATION

To my parents and brother, who supported me since the day I first saw the light of sun, who encouraged me on rainy days, who tolerated the agony of temporal and spatial separation, who understood without complaints the choices I made, and to whom I long to share joy with again.

ACKNOWLEDGMENTS

At the closure of a turbulent expedition, I feel grateful for so much help that I received over the years from people around me.

My utmost gratitude goes to my advisor, Dr. M. P. Soriaga. It is his exceptional generosity, unreserved help and invaluable advice over the years that made completion of this dissertation possible. I would also like to thank every member in my graduate committee, Dr. D. H. Russell, Dr. Y. Q. Gao, and Dr. D. Banerjee, who not only taught me chemistry but also toughened and inspired me in many different ways.

I would like to thank former and current members of the Soriaga research group: Dr. X. Chen, Dr. Y. S. Park, Dr. J. Sanabria, Dr. J. Baricuatro, Juan, Akhtar, Kyle, Miguel, and Alnald. These colleagues, good friends, have given me much needed assistance and also shared countless joyful moments in the past years.

I am deeply indebted to my family for their unending support.

This project was financially supported by The Welch Foundation.

TABLE OF CONTENTS

LIST OF FIGURES

Page

Page

Page

LIST OF TABLES

Page

CHAPTER I

INTRODUCTION

Background and Motivation

The catalytic properties of palladium have long been known to chemists and have been widely exploited in a variety of synthetic strategies over the past few decades. A good metal catalyst requires: (a) a weak intermetallic bond strength, to allow insertion of reactant between metal atoms, and (b) a not too strong metal-adsorbate interaction, to facilitate the desorption of reaction product.[1] Compared with other metals in the same group, Pd has the lowest metal-metal dissociation energy and bulk-to-vapor atomization enthalpy.[2] Therefore it is of no surprise that Pd is a robust catalyst for chemical reactions that involve the construction of carbon-carbon and carbon-heteroatom bonds.[3,4] Its highly selective catalytic activity is of importance in pharmaceutical, materials and biomolecular synthesis.[5-9] Its ability to absorb hydrogen into the bulk is also a desirable property especially for hydrogenation reactions as well as hydrogen storage.[10,11]

In terms of electrocatalysis by palladium surfaces, the electrode-electrolyte interface is of fundamental interest; also impacts related subfields such as heterogeneous catalysis, electrochemical processing, metal corrosion, batteries, and fuel cells. A thorough understanding of the mechanisms and dynamics of complex interfacial reactions must include a sound knowledge of the nature of the surface. While conventional electrochemistry is capable of providing thermodynamic and kinetic information, more advanced methodologies are required to obtain microscopic understanding of the surface

---

This dissertation follows the style of the *Journal of American Chemical Society*.

processes. Recent advances in the integration of modern surface analysis with fundamental electrochemical methods have allowed atomic-level information about phenomena at the electrode-electrolyte interface. Such phenomena, which include the nature of surface chemical bond, the orientation of the chemisorbed molecule, and the relative binding strengths of different functional groups, have been explored in this work.

In particular, this dissertation research is focused on the interaction of aromatic molecules with well-defined palladium electrode surfaces. Aromatic molecules are the model compounds; specifically dihydroxybenzene (hydroquinone) and its derivatives because of inherent electrochemical redox reactions that allow detailed interrogations based on classical electrochemical methods. The list of selected compounds is presented in the experimental section below.

Prior Work

Benzene

Previous studies with benzene at Pd(111) surfaces in our laboratory included electrochemistry, scanning tunneling microscopy (STM) and electron spectroscopies.[12] Among other surface-chemical aspects, it was found that, at low concentrations and at potentials within the double-layer region, the adsorbed benzene molecules adopt a Pd(111)-c($2\sqrt{3} \times \sqrt{3}$)-rect-$C_6H_6$ adlattice (Figure 1). As can be discerned in Figure 1, the adlayer is slightly tilted with respect to the substrate surface. Figure 2 shows the corresponding high resolution electron energy loss (HREEL) spectrum. The peaks were assigned as follows: (a) and (b) are from direct metal-adsorbate (Pd-C) chemical bonds; (c) and (d) are out-of-plane C-H bending; (e) and (i) are in-plane C-H stretching; (f) and (g) are in-plane bending. It is also worth noting that, at potentials just prior to the

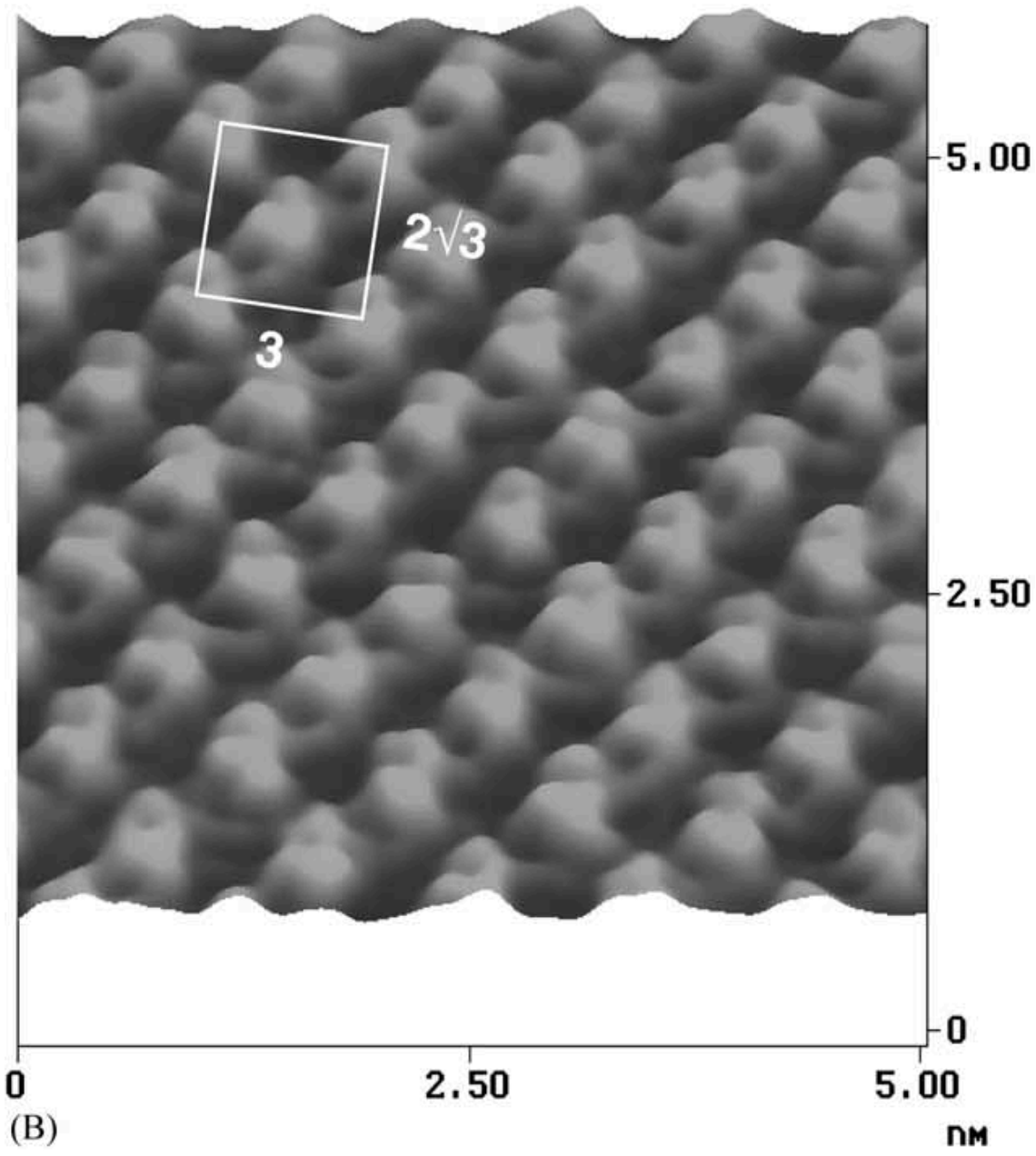

Figure 1. EC-STM image of Pd(111)-c($2\sqrt{3} \times \sqrt{3}$)-rect-C_6H_6 adlattice prepared from a dilute solution of benzene at potential within the double-layer potential.

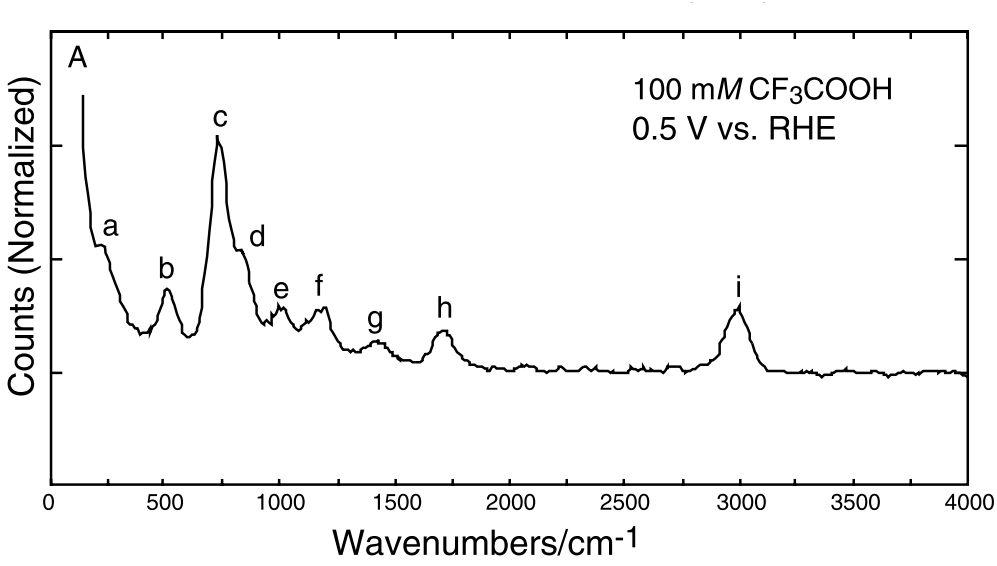

Figure 2. HREEL spectrum of chemisorbed benzene on Pd(111) at 0.5 V (vs. RHE) from a solution that contained 1 mM benzene in 100 mM tetrafluoroacetic acid.

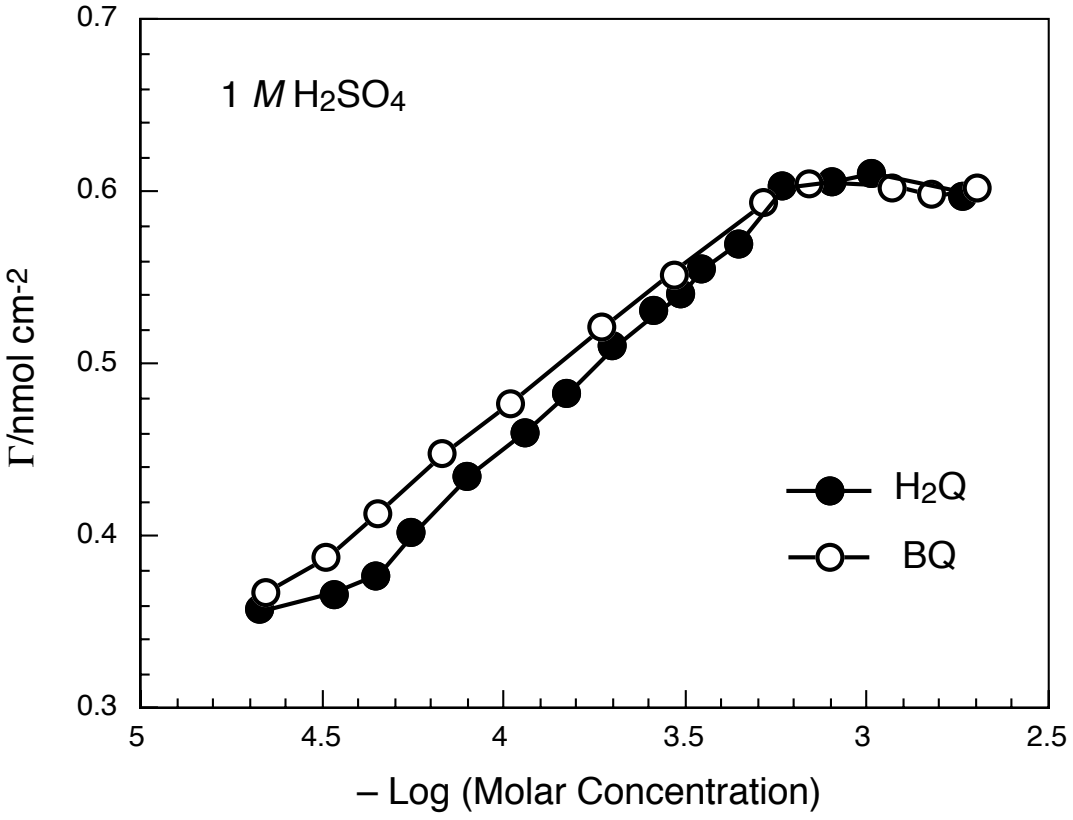

Figure 3. Chemisorption isotherm of hydroquinone and benzoquinone at polycrystalline Pd surfaces as measured by TLE.

hydrogen evolution region, the benzene adlayer is reconstructed into Pd(111)-(3×3)-C_6H_6 reversibly.

Hydroquinone

The surface chemical properties of hydroquinone on palladium single crystals have also been previously studied. [13-16]

Figure 3 shows the chemisorption isotherms for hydroquinone and benzoquinone as measured by thin layer electrochemistry (TLE). The near-identity between these two molecules is obvious. At concentrations lower than 0.1 mM, both molecules assume a flat orientation (η^6), indicating the strong interaction between the aromatic π-system and metal surface. At concentrations higher than 1 mM, both molecules adopt an edge-wise orientation (η^2), indicating Pd-C bonds at the 2,3 positions.

Figure 4 shows the STM image of 0.1 mM hydroquinone chemisorbed at a potential within the double-layer region. It is known that hydroquinone molecules oxidatively chemisorb on palladium surfaces in the flat orientation.[13] Therefore, the adlayer consists of benzoquinone instead of diphenol and displays a 3×3 structure. As can also be seen from the picture, the chemisorbed benzoquinone molecule, which is predominantly oriented flat on the surface, is slightly tilted with the 1,2 positions slightly closer to the surface than the 4,5 positions. It is also important to note that the formation of an ordered adlayer can be achieved within 2 minutes for hydroquinone,[14] while it takes 3-10 minutes to establish long range order for benzene, although diffusion effect may also have a role in the slow kinetics.[12]

Figure 5 shows the HREELS spectra of chemisorbed hydroquinone from solutions of various concentrations on Pd(100) surfaces. These spectra are similar to benzene except for the presence of the C=O stretching mode at 1480 cm^{-1}. To identify the orientation transition as was observed in the case of TLE, the normalized out-of-plane bending mode γ(CH) and in-plane stretching mode ν(CH) peak intensities were plotted as in Figure 6. It can be seen that ν(CH) remains largely unchanged over the entire concentration range. The normalization method used by this work, which will be explained in the experimental section later, elevates the impact-scattering-dominated region (2100 cm^{-1} to 2700 cm^{-1}) to the comparable level as the dipole-scattering regions. The postulate is that ν(CH) is largely dominated by impact scattering. This is further supported by off-specular studies of benzene on Pd(100).[17] γ(CH), on the other hand, displays a smooth transitional increment over the concentration range. Therefore the intensity ratio between γ(CH) and ν(CH) may serve as a sensitive probe to monitor changes in orientation of the chemisorbed molecules.

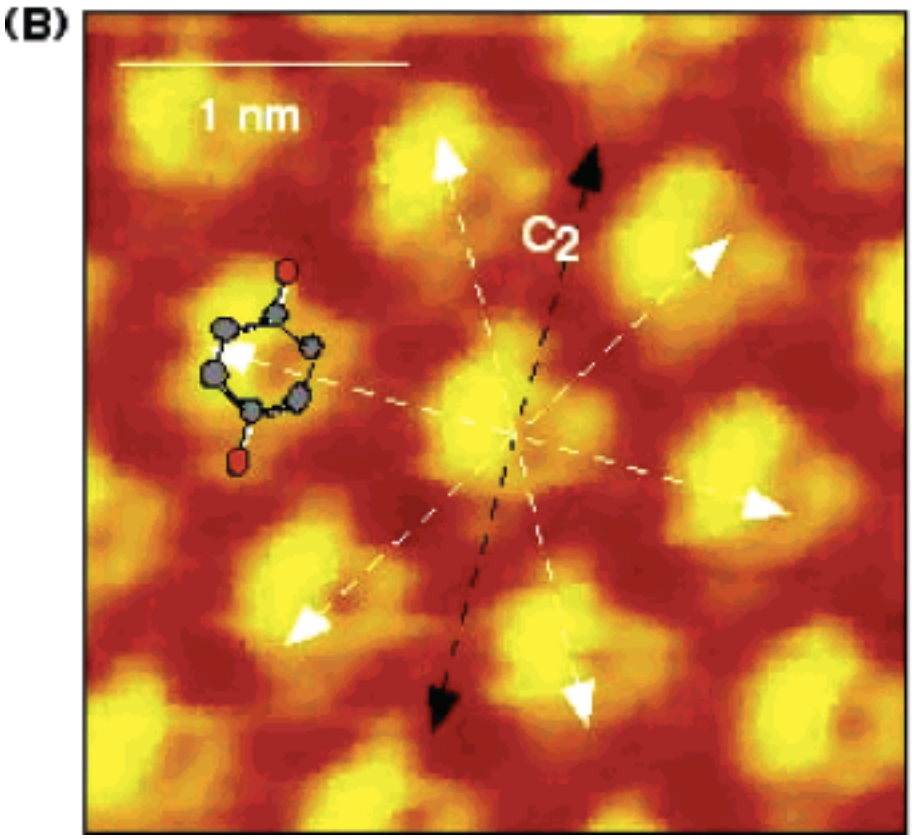

Figure 4. EC-STM image of a (3×3) adlayer of BQ on a Pd(111) surface.

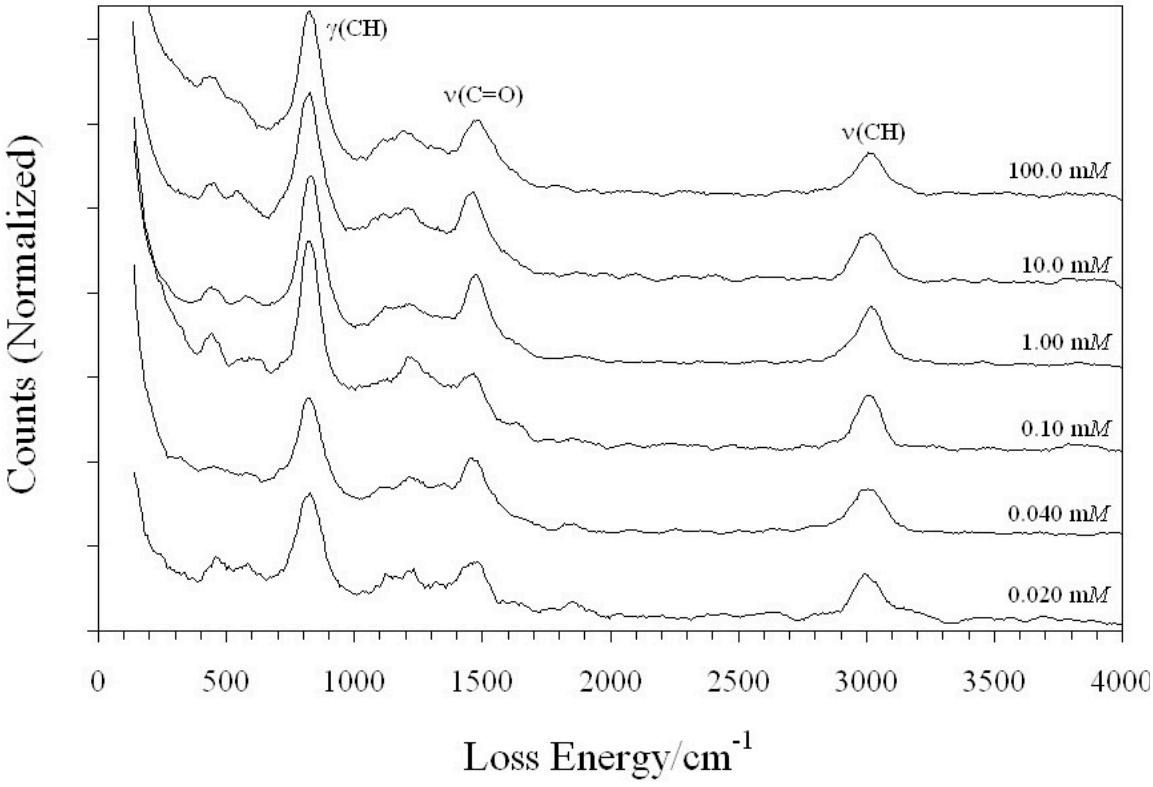

Figure 5. HREEL spectra of chemisorbed hydroquinone (as benzoquinone) on Pd(100) surfaces prepared from various concentrations.

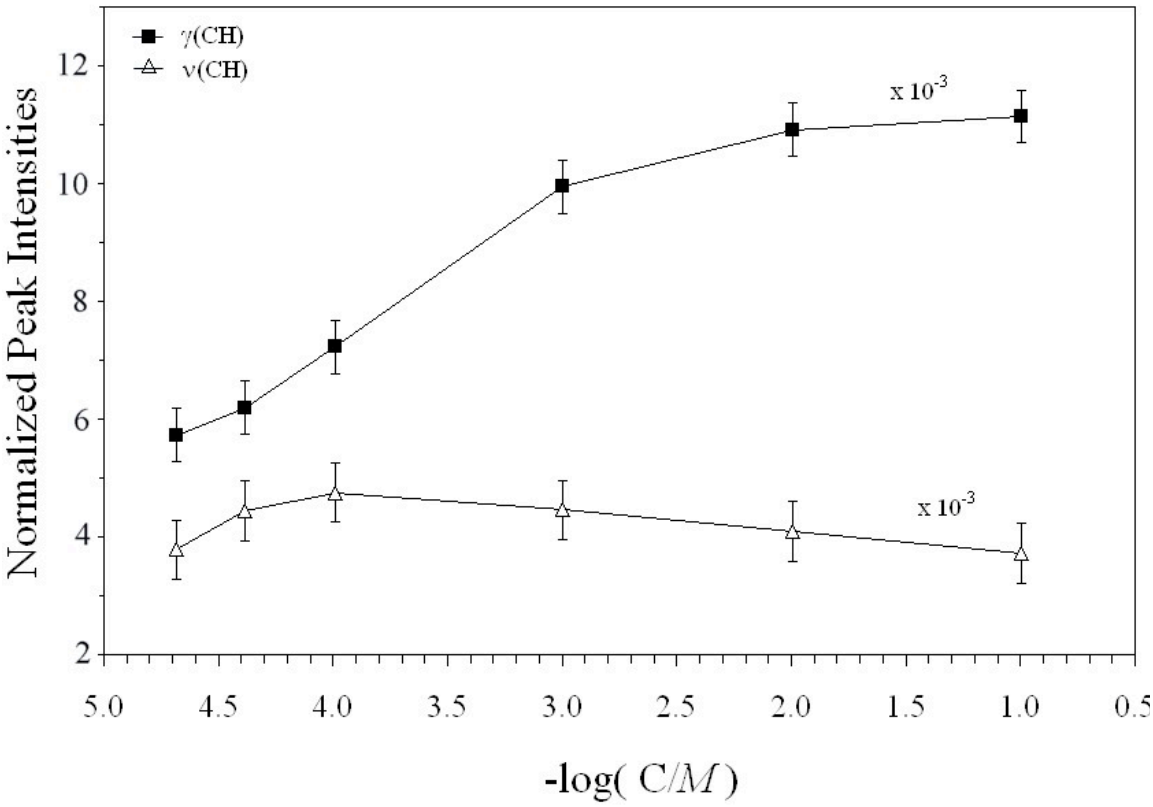

Figure 6. Normalized HREELS γ(CH) and ν(CH) peak intensities as a function of solution hydroquinone concentration.

CHAPTER II

EXPERIMENTAL

Thin Layer Electrochemistry (TLE)

Thin layer electrochemistry has been utilized extensively to survey the chemisorption properties (e.g., surface packing density and adsorbate molecular orientation) of organic molecules. The effectiveness of TLE owes to the following favorable aspects: (a) Elimination of mass transfer complications: the analyte solution is isolated in a thin-layer (25 μm) cavity. (b) Inhibition of contamination: This is due to the fact that only a small portion (~ 4μL) of solution is accessed in the thin-layer cavity. (c) Enhancement of surface reactions: This arises because of high surface area-to-volume ratio[18].

A schematic illustration of a thin-layer electrochemical cell is shown in Figure 7a. An H-cell serves to separate the working electrode from the reference electrode in order to minimize Cl^- ion contamination. The counter electrode is made of Pt wire, which is wrapped around the reference electrode. Figure 7b shows an enhanced view of the working electrode and the thin layer cavity. The distance between the Pd electrode surface and the cavity wall is less than 25 μm. To introduce solution inside the cavity, the tip of the cell, which contains two extremely small pinholes is simply immersed just below the solution level. Solution will fill up to the top of cavity without overflow due to a capillary effect. To remove the spent solution inside the cavity, N_2 gas is blown through the cell.

Electrode Surface Area

The surface roughness of thermally annealed Pd electrode is estimated to be 5%[19]. The active surface area of the clean Pd electrode is simply taken as the geometric area plus the 5% roughness factor:

$$Area = (2\pi r + \pi r^2) \times 1.05 \quad (1)$$

where r is the radius of the cylindrical Pd billet and L is the length. In this manner, the electrode surface area was measured to be 1.19 cm^2.*

Thin-layer Cell Volume

The volume (V) of the thin-layer cavity was determined from the equation below:

$$V = \frac{Q - Q_b}{nFC^o} \quad (2)$$

Here Q is the electrolytic charge of reduction or oxidation of selected redox couple, measured by potential-step coulometry. Q_b is the background charge in pure supporting electrolyte, F is the Faraday's constant and C^0 is the concentration of the redox-active species in solution.

The redox reaction of Fe^{2+}/Fe^{3+}

$$Fe^{3+} + e \rightleftharpoons Fe^{2+}$$

was used as an electrochemical probe to determine thin-layer cell volume since iron atoms do not chemisorb on the electrode surface.

* Electrochemical methods have been utilized to determine active surface area of Pt (through H adsorption) and Au (through I adsorption). However, these methods are not applicable to determine active surface area of Pd.

In this work, V was determined to be 3.60 μL; this value is typical of thin-layer cell.[19,20]

Determination of Surface Packing Density

TLE has been used to measure the surface packing density of chemisorbed molecules, in turn, the packing density has been explored to deduct the adsorbed molecule cross-section, a parameter that is directly related to adsorbed-molecule orientation.

(a) If the adsorbed molecule exhibits redox activity, the following equation was to measure surface coverage

$$\Gamma = \frac{Q - Q_b}{nFA} \tag{3}$$

where Q is electrolytic charge after the surface is saturated with chemisorbed species, which is obtained in blank electrolyte solution in the absence of analyte in solution. Q_b is the background electrolytic charge (the electrode surface is saturated with an structurally similar molecule to analyte, which does not exhibit redox activity). n is the number of electrons transferred per unit reaction. A is the electrode surface area.

(b) If the electrochemical activity is not preserved, the following equation was employed to determine surface coverage Γ:

$$\Gamma = \frac{(Q_2 - Q_{2b}) - (Q_1 - Q_{1b})}{nFA} \tag{4}$$

Herein Q_2 is the electrolytic charge of the second aliquot of filling with analyte in solution. Q_{2b} is the background charge of a second aliquot with the absence of analyte in solution. Q_1 is the electrolytic charge of the first aliquot of filling with analyte in

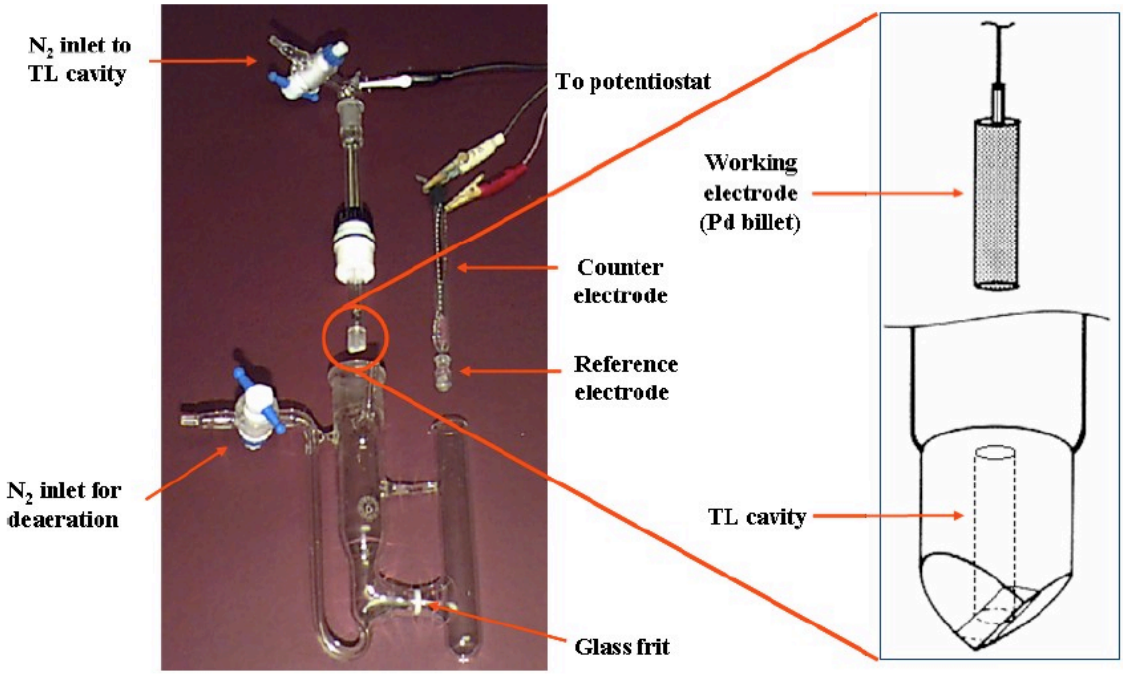

Figure 7. (a) Picture of a thin-layer electrochemical cell mounted in an H-cell; (b) Enhanced view of thin-layer cell cavity.

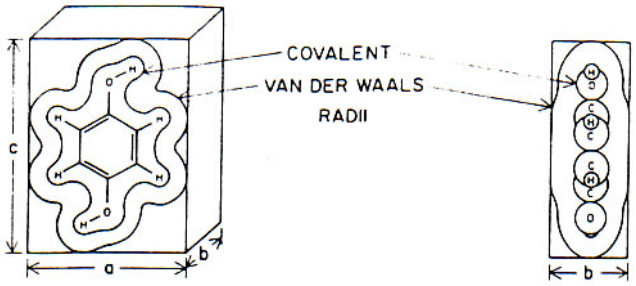

Figure 8. Molecular unit cell employed to determine adsorbed-molecule cross-section (area).

solution. Q_{1b} is the background charge of the first aliquot with the absence of analyte in solution. The assumption here is the electrode surface is saturated after the first aliquot.

Determination of Adsorbed-molecule Cross-section

The methodology to arrive at molecular cross-sections (and, hence, molecular orientations) is based upon a calculation procedure initially suggested by Paling that makes use of covalent and van der Waals radii[21-23]. As shown in Figure 8, the adsorbed molecule is modeled as a rectangular slab, the dimensions of which are determined by the van der Waals envelope of the molecule. The cross-section or average area σ (Å) per molecule is obtained from Γ (mole/cm^2) according to:

$$\sigma = \frac{10^{16}}{6.023 \times 10^{23} \Gamma} \tag{5}$$

There are usually three orientations for chemisorbed aromatic compounds: "flat" orientation (η^6) when all six aromatic carbon atoms are in close proximity to substrate; "edgewise" orientation (η^2) when one edge is parallel to substrate with the ring perpendicular to surface; "endwise" orientation (η^1) when a C-H bond of the ring is normal to surface.

Electron Spectroscopy (ES)

A comprehensive description of the electrode-electrolyte system depends on the determination of several parameters, these include solvent, electrolyte, electrode potential, surface electronic structure, crystallographic orientation and the surface activity of reactants. Purely electrochemical methods are far from sufficient to access these parameters. The absence of atomic-level specificity in traditional electrochemical methods leads to ambiguities. The desire for atomic-level understanding necessitates

these experimental mandates: (a) compositionally pure and structurally well characterized starting materials, (b) detailed structural and compositional analysis of important surface intermediates, (c) identification and subsequent quantitative analysis of the reaction product distributions. To satisfy these demands, it is of no surprise that most surface electrochemical studies focus on single crystal electrodes and employ surface sensitive analytical methods. Most surface sensitive techniques utilize electrons, ions, photons or tunneling currents as probes. In the present study, electrons are the probe of choice for all the surface-sensitive analytical techniques.

In ES, a solid surface is subjected to a beam of electrons of incident or primary energy E_p; this results in elastically backscattered (primary) and inelastically emitted (secondary) electrons. The resulting energy distribution, a plot of the number of electrons N(E) as a function of energy E, of these electrons is depicted in Figure 9. This spectrum can be divided into four regions according to the origin of the scattered electrons:

(a) True secondary electrons located in the low-energy range and are created as a result of multiple inelastic collisions between the incident electrons and those from surface. Due to the complexity of the formation mechanism, analysis based on this region is rare.

(b) The high-energy tail of the true secondary peak is actually accompanied by very weak peaks. The origins of these peaks are Auger electrons. These form the base of Auger electron spectroscopy.

(c) Primary electrons scattered without loss in energy. These elastically scattered electrons are monochromatic and form the basis of low energy electron diffraction.

(d) Just before the elastically scattered peak are very weak signals. The origins of these peaks are energy losses associated with vibrational modes at the sample surface; at high-resolution, these peaks can be used for surface vibrational spectroscopy.

Techniques that make use of electrons require high vacuum (< 10^{-7} torr) to avoid loss of electrons and/or collision-induced spectral complications. Ultrahigh vacuum (UHV) conditions not only satisfy this demand, but also ensure minimal contamination to the sample surfaces. Under UHV condition, the mean free path for gas molecules is exceedingly large (10^5 m).

Instrumentation

Figure 10 shows the all stainless-steel UHV instrument employed in this research. The apparatus utilizes a three-stage pumping. Two liquid-nitrogen chilled adsorption pumps (MS-5A-23, Duniway) first reduce pressure from ambient pressure to 10^{-3} torr. A 56 L/s turbo pump (TPU 060, Pfeiffer) further decreases pressure to 10^{-7} torr. Finally, a 300 L/s ion pump (TNB-X 500, Perkin Elmer) then functions as the last stage to maintain pressure below10^{-8} torr.

The ES-Electrochemistry apparatus consists of two compartments: the electrochemistry (EC) and electron spectroscopy (ES) chambers. An X-Y-Z-R manipulator (Huntington Laboratories, Mountain View, CA), installed on a twin-rail positioning table, allows the transfer of the crystal from the ES chamber to the EC chamber. A gate-valve (MDC Vacuum Products, Hayward, CA) allows the isolation of the ES chamber when EC experiments are being performed at atmospheric pressure in EC chamber. The ES chamber is equipped with (a) LEED optics (15-120, Perkin-Elmer) for surface structure analysis, (b) AES optics (10-155, Perkin-Elmer) for elemental

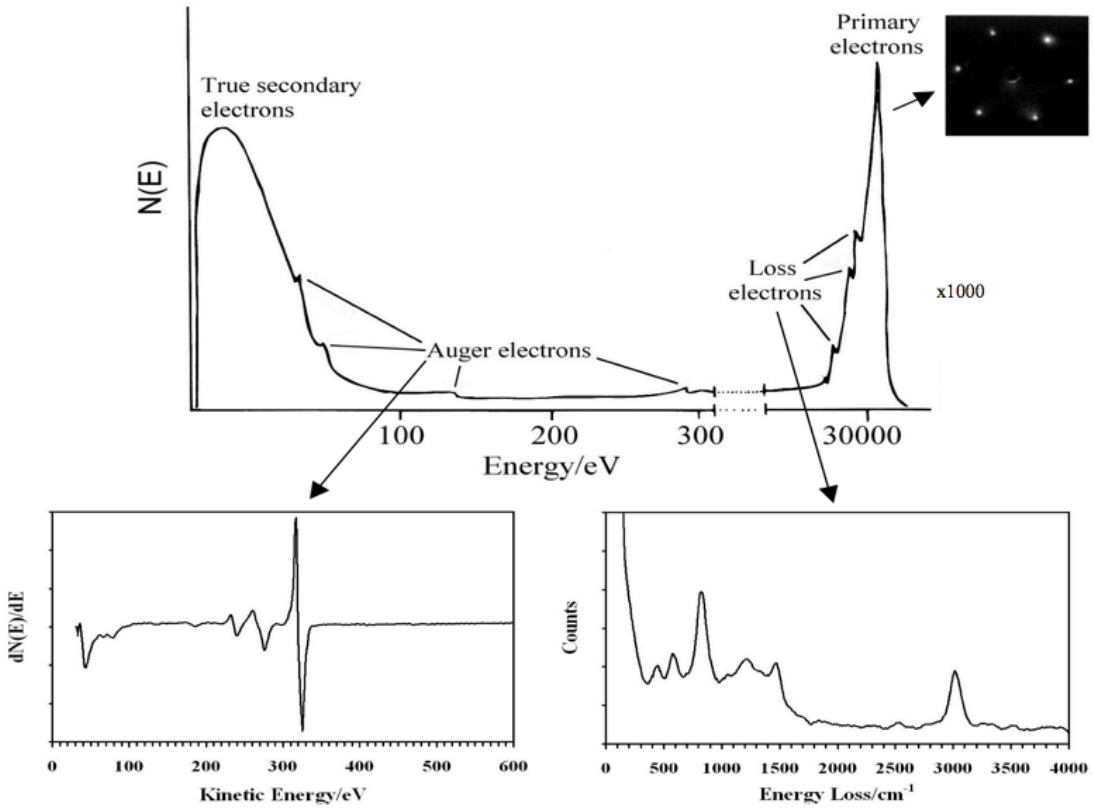

Figure 9. Energy distribution of scattered electron in various electron spectroscopy.

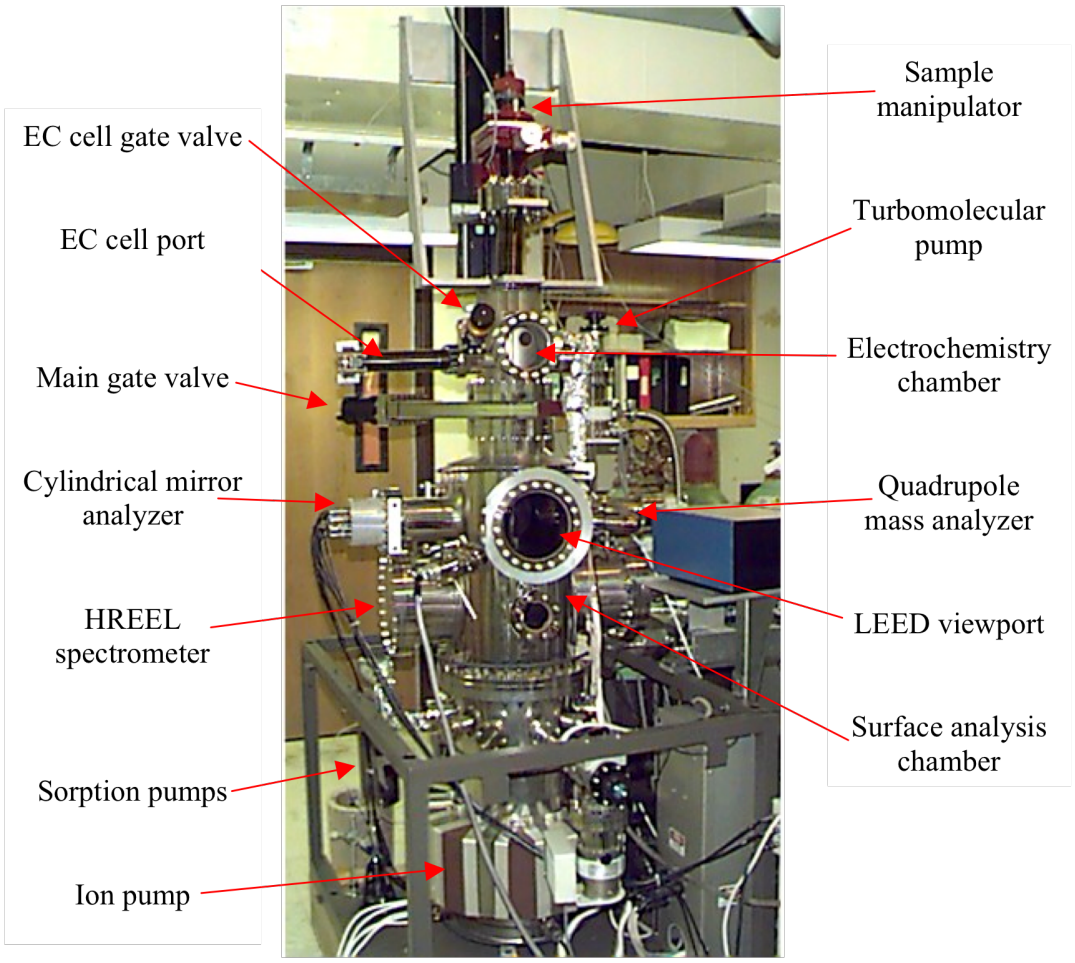

Figure 10. Picture of ES-EC apparatus.

detection of the surface, (c) HREELS optics (LK 2000, LK Technologies) for vibrational spectroscopic information. A 72-hour of bakeout of the entire apparatus at 475 K is carried out when residual pressure inside the chamber stays above 10^{-8} torr.

Low Energy Electron Diffraction (LEED)

Single crystals are extensively studied in UHV systems to minimize reaction complexity, since different faces usually lead to different activation energy of reaction. LEED is a fast and non-destructive technique to confirm long-range surface order and smoothness. In LEED, a monochromatic beam of low-energy electrons is impinged onto a surface and the elastically backscattered electrons are collected on a phosphor screen. There are a few features of LEED that needs to be mentioned: (a) The electron energy must be such that the electron mean free path (Figure 11) is at a minimum to grant LEED its surface sensitivity.[24] (b) For diffraction to occur on a lattice with crystal lattice dimensions on the magnitude of angstroms, an electron beam energy of 30 - 80 eV is desired ($U = 0.015/d^2$, here U is electron energy in eV, d is inter-atomic distance in Å). In this work, a LEED energy of 48 eV was used. (c) The backscattering yield is highest when the electron beam energy lies in this region. (d) The coherence width of electron beam source in LEED is typically 100 angstrom. To obtain a sharp LEED pattern, a minimum area of 100 x 100 $Å^2$ of continuous well-ordered domain is required. [25]

To understand and analyze LEED patterns, one takes advantage of the well-known wave and particle duality nature of electrons. As waves scattered at an array periodic in one-dimension, constructive interference occurs when adjacent scattered waves have path difference that are integral multiples of the wavelength λ (Figure 12a).

$$a(\sin\varphi - \sin\varphi_0) = n\lambda \qquad (6)$$

Here, a is the distance between adjacent scatters (metal atoms). φ_0 is the angle of the incident wave, φ is the angle of diffraction wave. In LEED, $\varphi_0 = 0$, thus $\sin\varphi_0 = 0$. To denote the fact that the diffraction patterns represent the reciprocal of the real-space order, equation (6) is typically rewritten in terms of Miller indices (hk) in two dimensions:

$$n\lambda = d_{hk}\sin\theta_{hk} \tag{7}$$

In equation (7), d_{hk} and θ_{hk} are the distance between scatters, and diffraction maximum angle in the direction of (hk)[26]. d_{hk} is related to real space atomic pattern and θ_{hk} is related to the diffracted pattern. It is obvious, in Figure 12b, that large crystal lattice parameters lead to more a closely packed LEED pattern.

In real space, the overlayer is represented as

$$b = M \bullet a = \begin{pmatrix} m_{11} & m_{12} \\ m_{21} & m_{22} \end{pmatrix} \bullet a \tag{8}$$

Here, a is the matrix representation of substrate mesh, in detail $a = \begin{pmatrix} a_1 \\ a_2 \end{pmatrix}$, b is the matrix representation of the overlayer mesh, in detail $b = \begin{pmatrix} b_1 \\ b_2 \end{pmatrix}$.

The reciprocal space representation shows a similar relationship

$$b^* = M^* \bullet a^* = \begin{pmatrix} m_{11}^* & m_{12}^* \\ m_{21}^* & m_{22}^* \end{pmatrix} \bullet a^* \tag{9}$$

It can be shown that M^* is the inverse transpose of M, thus

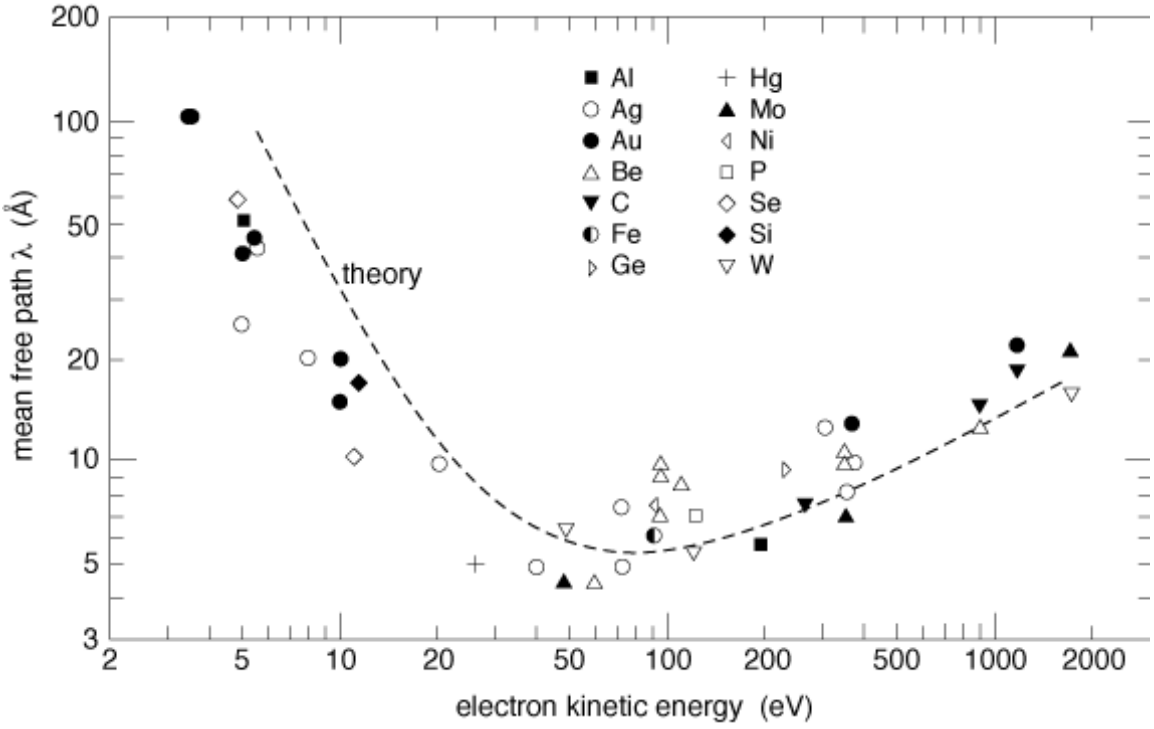

Figure 11. “Universal curve”: Mean free path of electrons in solid.

a.

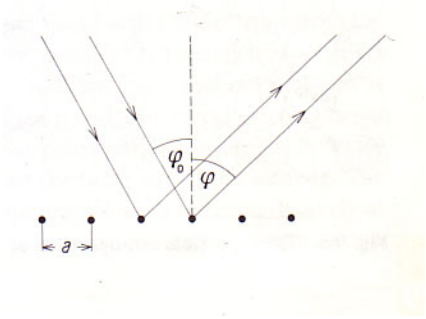

b.

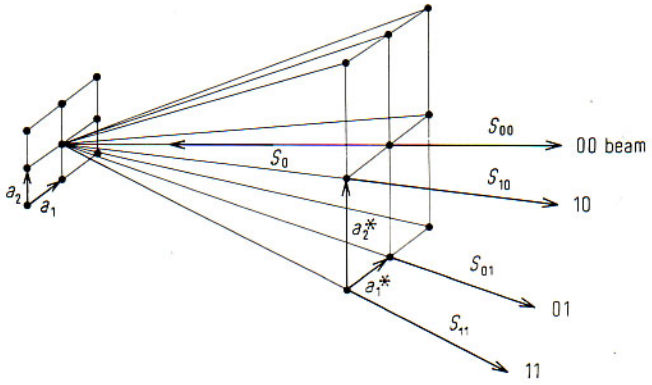

Figure 12. Principle of the formation of a) 1-D and b) 2-D LEED patterns.

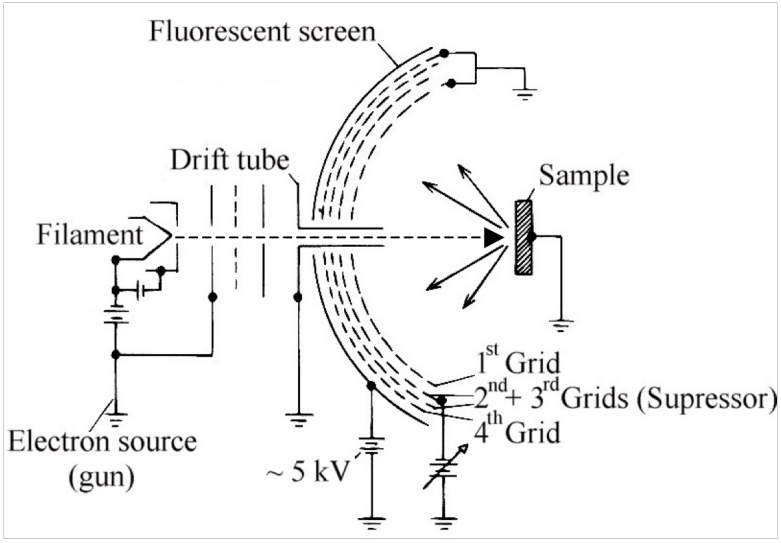

Figure 13. Schematic diagram of LEED apparatus.

$$
\begin{aligned}
m_{11} &= \frac{1}{\det M^*} m_{22}^* \\
m_{12} &= \frac{1}{\det M^*} m_{21}^* \\
m_{21} &= \frac{1}{\det M^*} m_{12}^* \\
m_{22} &= \frac{1}{\det M^*} m_{11}^*
\end{aligned}
\tag{10}
$$

It may be recalled that the determinant of a two-by-two matrix M^* is

$$\det M^* = m_{11}^* m_{22}^* - m_{21}^* m_{12}^* \tag{11}$$

The above equations allow the real surface lattice to be constructed from the corresponding LEED (reciprocal-space) patterns.[27,28]

Figure 13 shows the schematic diagram of the LEED electron optics. An electron beam generated from a hot filament (tungsten) is focused by several slits. This beam is then irradiated onto the metal surface. Inelastically backscattered electrons are filtered out through application of retarding grids. The remaining elastically scattered electrons are accelerated to induce fluorescence on a phosphor coated hemispherical screen.

Auger Electron Spectroscopy (AES)

AES is a widely used technique for surface elemental analysis. The creation of an Auger electron involves three steps. First an electron at the core level of the element of interest is ejected by a highly energetic source (usually, as is the case in this work, electrons)[27]. Then, this vacated energy level is immediately filled by an electron at a higher energy, a process that still leaves the atom in an excited state. The final relaxation process releases a second electron (Auger electron). The notation for an Auger process can be gleaned from Figure 14, for a KL_1L_3 transition. The energy of a KL_1L_3 transition is given by

$$E_{KL1L3} = E_K - E_{L1} - E_{L3} - \phi_{sp} \quad (12)$$

If the sample and spectrometer share the same Fermi level (i. e., in good contact), the observed Auger electron kinetic energy must include the spectrometer work function ϕ_{sp}.

The energy of Auger transitions is usually convoluted by many electron effects and final state energy variations[29] such as multiple scattering, and the energy lost in the form of plasmon, *etc*. Differentiation of the spectra is frequently employed to enhance the weak Auger signal from the intense secondary-electron spectral background. A software library is used to assist in the identification of surface elements.

A schematic diagram of the PE 10-155 cylindrical mirror analyzer (CMA) (Perkin Elmer) used in the present work is given in Figure 15. Energy analysis with a CMA is achieved by applying a negative ramp voltage (V) to the outer cylinder while the inner cylinder is held at ground. Only electrons of the appropriate energy can pass unhindered through the CMA and onto the detector, a channel electron multiplier. The pass energy of the CMA is modulated and then synchronously demodulated via a lock-in amplifier to acquire the derivative spectrum. The resolution of a CMA is dependent upon its entrance and exit slits; improved resolution can be achieved by a double-pass CMA. Since the Auger process is an inelastic process, a wide emission angle is expected. This is in contrast to elastic processes, which occur exclusively at the specular angle.

Quantification of the AES signal has been discussed extensively[27,30-32]. AES is not well suited for precise quantitative analysis and a semi-quantitative procedure employed enables the adsorbate packing density Γ_a to be calculated in a simple manner.

$$\Gamma_a = \left(\frac{I_a}{I^0{}_M}\right)\frac{1}{B_a} \quad (13)$$

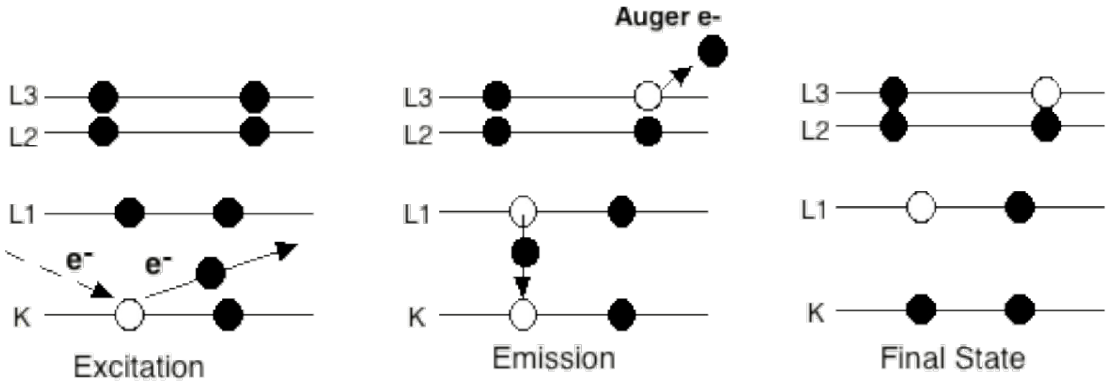

Figure 14. Schematic diagram of Auger electron generation.

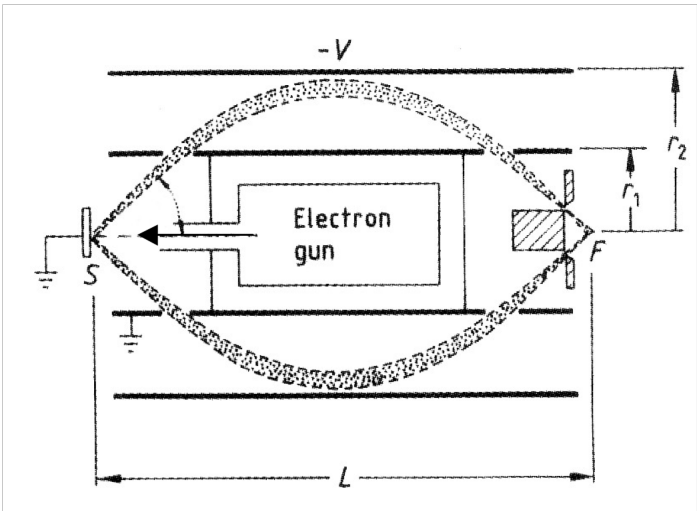

Figure 15. Schematic diagram of a cylindrical mirror analyzer. L is the distance between sample and detector; r_1 and r_2 are the radii for inner and outer cylinders respectively; V is the ramp voltage.

Here, I_a and I^0_M are the Auger currents of the adsorbed species and clean metal substrate respectively. B_a is the calibration factor, which is based upon independent means of coverage measurement.[33,34]

High Resolution Electron Energy Loss Spectroscopy (HREELS)

Most electrons incident at a solid surface undergo inelastic events, which causes them to be backscattered at energies lower than their initial energy or primary energy E_p. If E_l is the energy lost to the surface, the scattered electrons would have energy at $\Delta E = E_p - E_l$. The backscattered-electron spectrum then consists of peaks that arise from electrons that have suffered energy losses. Such peaks, commonly referred to as energy-loss peaks, originate from core-level ionizations, valence-level excitation, plasmon losses, phonon losses or vibrational excitations[1,28]. For low-energy incident electrons (2-10 eV) as the case of HREELS, the loss of energy corresponds to surface-vibration at energies that usually lie in the energy range below 4000 cm^{-1} (or 0.50 eV, since 1 meV = 8 cm^{-1}). A typical HREELS instrument yields a resolution of 32 cm^{-1} or 4 meV, although more expensive models[35] claim to have resolution as low as 4 cm^{-1}. The limit of detection for strong dipole scatterers such as CO can be as low as 0.0001 monolayer. For weak scatterers such as hydrogen, the limit of detection is 0.01 monolayer. Given these properties, HREELS is an extremely sensitive technique for surface analysis, much more sensitive than infrared reflection adsorption spectroscopy.[36]

Three mechanisms give rise to HREELS spectra[27,28,37-39]: dipole scattering, impact scattering and negative ion resonance.

In dipole scattering, the incident electron may be treated as an electromagnetic wave that interacts, at a long range (d ≈ 60 Å),[28] with oscillating dipoles at the surface.

Dipole-scattering HREELS may thus be described in terms of the harmonic-oscillator vibrational selection rules: at ambient temperatures: (a) only fundamental transitions (ν=0 to ν=1, where ν is the vibrational quantum number) are allowed and (b) only vibrations accompanied by a change in dipole moment are observed. On metal surfaces, two additional selection rules apply. The first is that only vibrations with components normal to surface are HREELS active. This rule follows from two phenomena unique at metal surfaces: (a) These electromagnetic fields polarized perpendicular to the plane of incidence (i.e., parallel to the plane of surface) undergo a 180° phase-shift upon reflection. Consequently, at the point of incident, the electric-field vectors of the incident and reflected waves cancel each other. Hence, no field exists that can couple with dipoles that oscillate parallel to the surface. (b) Due to the formation of image-charges on metal surfaces, the dynamic dipole moment generated by an oscillator that vibrates in the surface-parallel direction is cancelled by that of its image dipole (Figure 16). The net dynamic dipole moment is zero and thus not HREELS active. On the other hand, if the real dipole is oriented perpendicularly to the surface, its dynamic dipole moment is enhanced by that of its image dipole. The second dipole scattering selection rule states that the intensity is at a maximum when the angle of collection is the same as the angle of specular reflection. This is illustrated in Figure 17. The intensity of the dipole scattered peak at 130 meV falls drastically as soon as the collection angle deviates from the specular angle. It is worth noting that angular dependence of the elastic peak is the same as that of the dipole-scattered peak.

The mechanism of impact scattering at solids is rather complex as it involves the penetration of the incident electron into the adsorbed molecule. The theoretical treatment

requires a quantum mechanical formalism. The transfer of energy from the incident electron to a vibrational mode occurs, in short range (a few Å), while the electron is inside the molecule. The dipole scattering selection rules do not apply to impact scattering. Theoretical considerations have predicted, and experimental studies have confirmed, the following "propensity rules" for this mechanism: (a) Usually, impact scattering vanishes in the specular direction. That is, impact scattered peaks can be observed only if detection is at angles removed from the specular direction. The dependence of impact scattering on the scattering angle, where θ is the deviation of the collection angle from the specular reflection, is shown in Figure 17. Impact scattering (80 meV) is most prominent when θ is close to 15°. (b) The probability of impact scattering (ρ) increases when incident electron energy (E_0) increases ($\rho \propto E_0$), whereas the dipole scattering probability has an inverse relationship to incident electron energy ($\rho \propto E_0^{-1}$).[40-42] (c) Strong dipole scatters are weak impact scatters; conversely, weak dipole scatters are strong impact scatters.

The last mechanism, negative-ion resonance, is beyond the scope of this study and will not be discussed further.

All three mechanisms co-exist in a given HREELS measurement, which introduce complications to data interpretation. However, it is possible to control experimental parameters to favor one of these three mechanisms. Dipole scattering is the dominant mechanism in the present study due to the following reasons: (a) The scattered electrons are collected at the specular angle where dipole scattering is the main contributor to peak counts. (b) Incident electron energy is adjusted to 3.6 eV, at which dipole scattering is favored over impact scattering. [37,43,44]

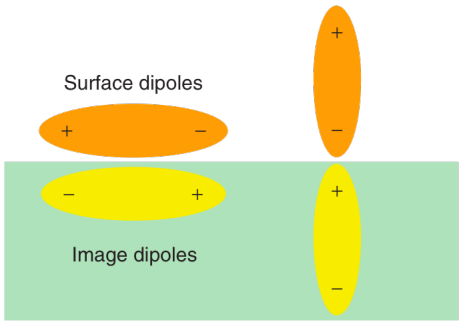

Figure 16. Illustration of the effect of the image dipoles on net oscillation at a metal surface.

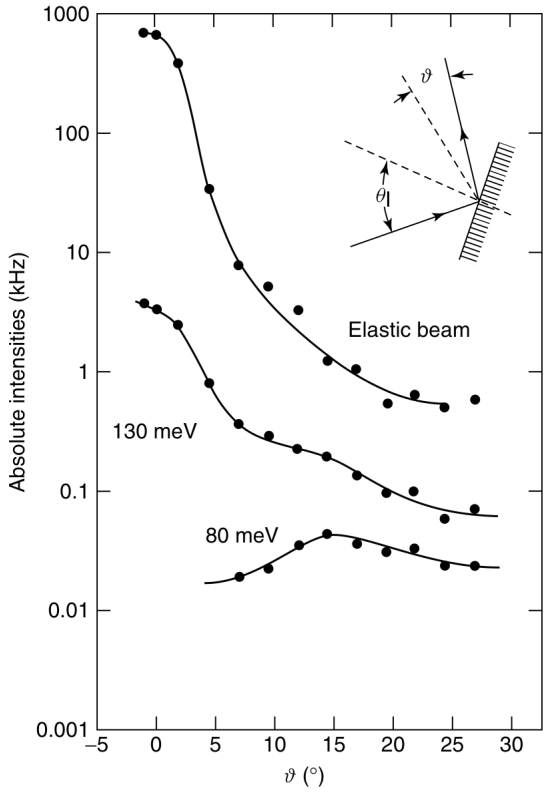

Figure 17. Angular distribution of impact scattering (80 meV), dipole scattering (130 meV) and elastic scattering in HREELS. θ_i is the incident angle. θ is the difference between specular angle and detector angle.

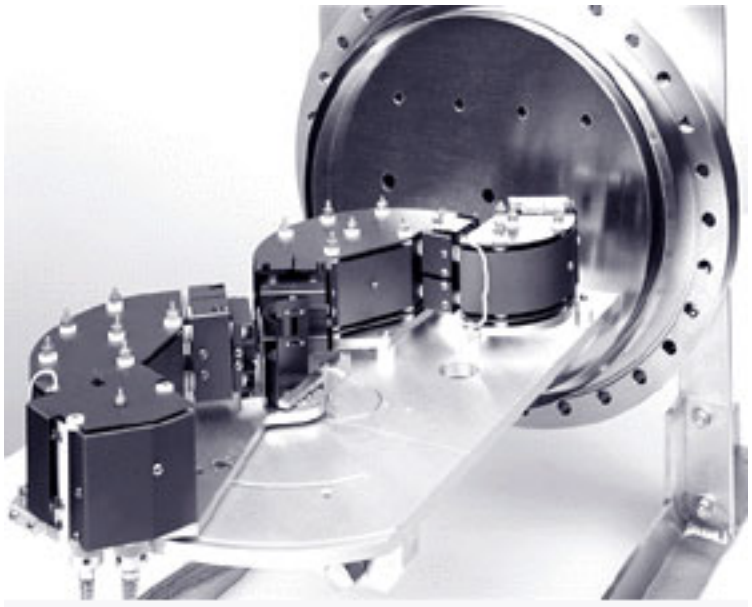

Figure 18. Picture of HREELS LK2000 apparatus.

Figure 18 shows a commercially available HREEL spectrometer, LK 2000. Off-specular collection of the backscattered electrons is afforded by rotation of either the sample or the analyzer. In the present study, no off-specular collection was obtained. This model consists of an electron gun (with LaB_6 as the filament), a two-stage monochromator, a single-stage energy analyzer, and a channel electron multiplier (channeltron) detector. Both energy monochromation and energy analysis are carried out with 127° cylindrical deflection analyzers. The incident electrons have an initial energy spread of 0.3 eV. The two- stage monochromator serves to narrow the energy spread to <1 meV and generate a highly monoenergetic beam of low-energy electrons (typically 1 to 10 eV).[35,45,46] The factory resolution was stated to be 4 meV (32 cm^{-1}), which was obtained on a highly ordered pyrolytic graphite (HOPG) surface. In the present study, on adsorbate-covered well-defined Pd(111) single crystal surfaces, the resolution was 5 ± 1 meV actually.

All spectra were normalized according to the following procedure: (a) a spectrum of a freshly prepared clean Pd crystal was collected and its elastic peak counts were proportionally adjusted to yield $2.5x10^5$ counts per second. This serves as a standard spectrum. (b) Each spectrum with adsorbed organic species was then multiplied by a ratio constant to normalize the background region of a spectrum (2100~2700 cm^{-1}) to that of the standard spectrum. This method assumes that the background region of a spectrum is mainly due to multiple and recombination losses which are enhanced by impact scattering.[47]

The shapes of the HREELS peaks in this study, have been taken to follow a Lorentzian distribution, which is typical of vibrational spectral peaks.

Numerical Computations

Density function theory (DFT) numerical calculation was carried out in this research to determine the preferential binding-site and adsorbed-molecule configuration. The DFT calculation employed was carried out with the Cambridge Sequential Total Energy Package (CASTEP), a first-principles code integrated in the Material Studio program (Accelrys Inc.).

The metal surface was represented by a slab that contained four layers of Pd atoms; only the upper two layers were allowed to re-construct. In this numerical simulation, lateral inter-adsorbate interactions have been excluded as the substrate studied was not densely packed.

The relative stability of various adsorption configurations were evaluated from the calculated adsorption energy, E_{ad}, given by:

$$E_{ads} = E_{Pd(111)-BQS} - (E_{BQS} + E_{Pd(111)})$$

where $E_{Pd(111)-BQS}$ represents the final-state energy after chemisorption, while E_{BQS} and $E_{Pd(111)}$ are the respective energies for initial state (the unbound) BQS and Pd(111).[48-53]

Samples and Reagents

Polycrystalline Pd Electrode

The polycrystalline palladium electrode used for TLE experiments was fabricated from a 99.99%-pure polycrystalline Pd rod (Wilkinson Co.). The electrode was metallographically polished, followed by fine-grade polishing with 1 micron and ¼ micron diamond paste (Buehler Ltd.). Prior to use, the electrode was thermally annealed

to about 1000 C° in a hydrogen-oxygen flame and quenched in N_2-saturated Milli-Q water (18 MΩ, Fisher Scientific).

Pd(111) Single Crystal

The crystallographically oriented Pd(111) single-crystal electrode (99.999 % purity) was purchased and polished (Materials Research Center, Cornell University, Ithaca, NY) prior to use. The sample was a circular disk: a diameter of 0.9 cm and thickness of 0.3 cm. Both faces of the disc were aligned to within 0.5° of the (111) crystallographic plane and were polished to a mirror finish. Although the edges were not oriented, they were metallographically polished also. The crystal was attached to the crystal holder via two 0.5 mm Pd wires (99.99%, Aldrich). These wires also allowed electrical contact thermal and electrochemical treatments. A Pt-10 % Rh/Pt thermocouple wire (Omega Engineering) was spot-welded to the top-edge of the crystal to monitor temperature.

Preparation of Pd(111) Single Crystal Under UHV Conditions

Cleaning of the Pd(111) single crystal was performed by a combination of the steps below: (a) Oxygen burning: thermal annealing at 1020 K in 3.0×10^{-5} torr of O_2 (99.8%) and (b) Ar^+ bombardment: Ar^+ ion sputtering (7.5 mA) at 5.5×10^{-5} torr of Ar (99.9999%). (c) Thermal annealing*:* maintaining temperature of crystal at 1020 K for 1 minute. Repeated steps above over years can disrupt surface smoothness, thus minimum steps were taken to clean crystal. Surface cleanness is verified by both AES and HREELS in the present study to ensure a purity level of > 0.99 monolayer of clean Pd.[45]

ES-EC Experiment Procedure

A typical ES-EC experiment follows these steps: (a) The Pd(111) substrate is

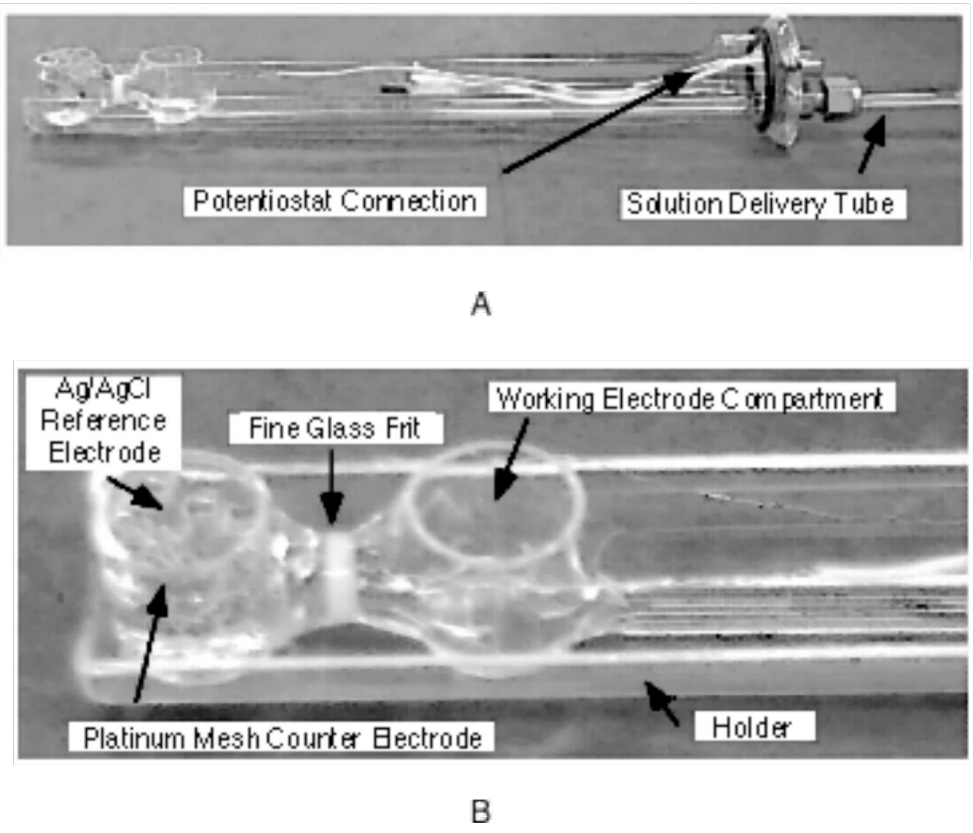

Figure 19. Picture of electrochemical cell used in the ES-EC study.

cleaned and characterized. (b) The single crystal is transferred to the EC chamber and isolated from the ES chamber by closing the gate valve between the two chambers. (c) Ultra-high-purity Argon (99.9999%) is then introduced into the EC chamber, and the EC-cell gate valve is opened to allow the insertion of the electrochemical cell. (d) The EC cell is filled with solution and the crystal is immersed completely below solution level. (e) After the EC experiment is completed, the crystal is emersed from the EC cell. (f) The EC chamber is pumped down to 10^{-7} torr, the gate valve is re-opened to allow the crystal to be transferred back to the ES chamber for further characterization.

Bake Out

To bake out, the entire chamber is wrapped with heating tapes then covered with glassy wool jackets. The temperature is maintained at approximately 475K for 72 hours. This measure is usually taken whenever the chamber is open for maintenance or internal pressure remains high (above 10^{-8} torr).

Electrochemistry

For the ES-EC studies, a custom-built cell was used as shown in Figure 19. The cell consisted of two 5-mL compartments separated by a fine glass frit: one contained the Pd(111) crystal (working electrode), the other one a Pt mesh (auxiliary electrode) and a reference electrode. The resistance of this cell, in a typical experiment, was determined to be 2 kΩ.

Both TLE and ES-ECexperiments employed the same potentiostat (CV-27, Bioanalytical Systems Inc.) and X-Y recorder (VP-6414S, Soltec). All potentials in this work refer to Ag/AgCl electrodes. In TLE, the Cl^- concentration was 1 M; while in ES-

EC, the Cl^- concentration was 1 mM. Plotted data was further processed by DigitizeIt™ software.

The H_2SO_4 supporting electrolyte solutions used in the TLE (1.0 M H_2SO_4) and ES-EC (10 mM H_2SO_4) experiments were prepared from fuming sulfuric acid (Aldrich Chemicals). Sodium carbonate (Mallinckrodt) was added to H_2SO_4 to yield a buffer of 10 mM HCO_3^- and 10 mM H_2CO_3 of pH=7. All solutions were made up with 18 MΩ resistance water (Milli-Q® Plus, Aldrich).

Selected Diphenolic Compounds

The selected aromatic compounds are shown in Figure 20, and the corresponding chemical names are listed in Table 1. Hydroquinone (**1**) was picked as the prototype aromatic due to its well-characterized electrochemical and spectrometric properties. 2,3-diphenolic hydroquinone (**2**) and 2,3,5-trimethyl hydroquinone (**3**) were selected to study the effect of methyl substituent. Hydroquinone sulfonic acid (as the potassium salt) (**4**) was chosen to evaluate the effect of a bulky sulfonate group. 1,4-dihydroxynaphthalene (**5**), anthraquinone-2-sulfonic acid (sodium salt) (**6**) and 2-phenylhydroquinone (**7**) were employed to study the effect of fused or pendant aromatic rings. 2,3-dihydroxypyridine (**8**) and 3,6-dihydroxypyridazine (**9**) were selected to investigate the effect of the nitrogen heteroatoms. 2,5-Dihydroxythiophenol (**10**) and 2-(8-mercaptooctyl)-1,4-Benzenediol (**11**) were chosen to evaluate the effect of short-chain and long-chain thiol group. Compounds **1**-**7** were purchased from Aldrich; **8** and **9** were purchased from Alfa Aesar. Compound **10** was synthesized according to the procedure below. Compound **11** was synthesized by Dr. Kurt V. Gothelf from the University of Aarhus.

Synthesis of 2,5-Dihydroxythiophenol (DHT)

The synthesis of DHT was based upon published procedure.[54] Twenty-six grams of benzoquinone (0.2 mol) was dissolved in 75 ml glacial acetic acid and heated to 40-50 °C. Seventy-five grams of sodium thiosulfate was dissolved in 100 mL water. The previously prepared benzoquinone solution was slowly added to sodium thiosulfate solution. This combined solution was stirred for 2 minutes. Potassium chloride (KCl) was then added to this mixture until copious amounts of white precipitate (2,5-Dihydroxyphenylthiosulfate) appeared. After 2 hours, the precipitate was filtered out and rinsed with concentrated KCl solution. The precipitate was then left in the dark to dry for 12 hours.

2.6 gram of 2,5-Dihydroxyphenylthiosulfate was dissolved in a mixture of 26 mL water and 20 mL concentrated HCl. 5 grams zinc powder was slowly added to the above solution. The temperature was carefully maintained at 40-50 °C. The product was extracted with ethyl ether at room temperature. The organic phase was poured on a Petri dish and transferred to a desiccator. Re-crystallization in benzene was applied to achieve higher purity. The final product was colorless crystalline needles. Mass spectrometry was used to determine that the purity of the synthesized DHT was at least 95%.

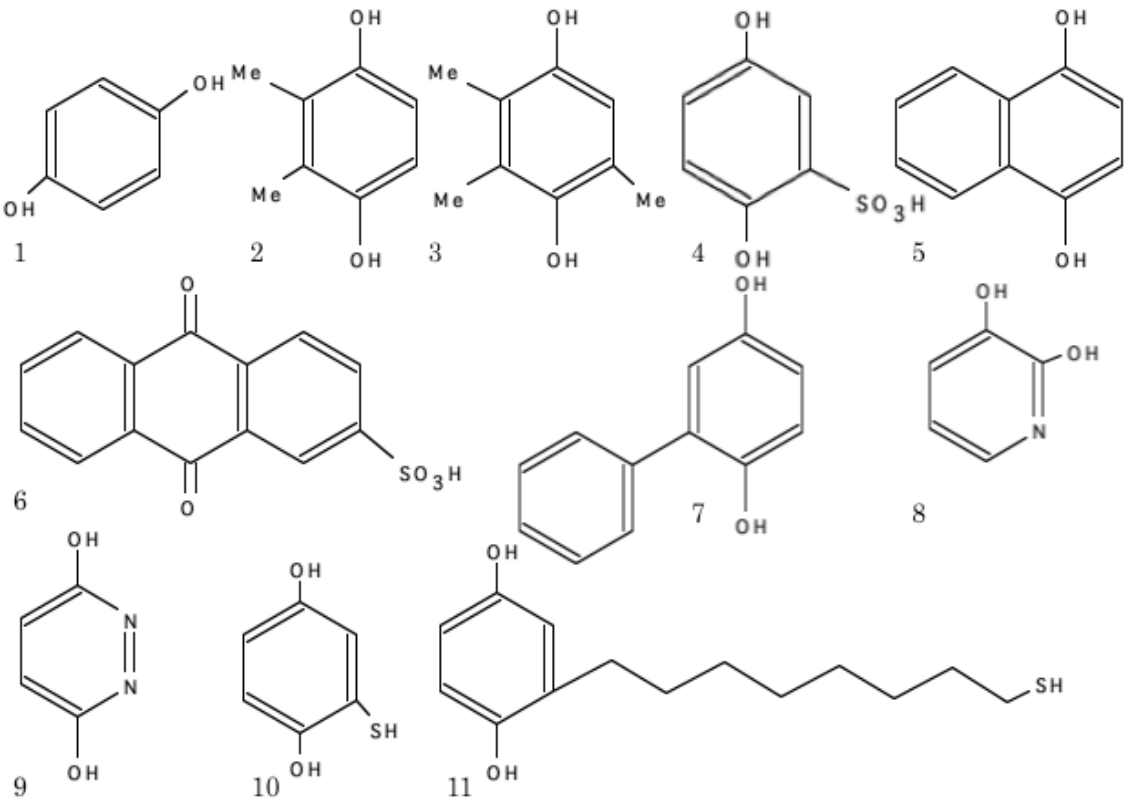

Figure 20. Structure of selected aromatic compounds.

Table 1. Selected aromatic compounds. These are the starting materials. The structure of which may not necessarily be the same as the chemisorbed species.

Compound Number	**Chemical Name**
1	hydroquinone (H_2Q)
2	2,3- diphenolichydroquinone
3	2,3,5-trimethylhydroquinone
4	hydroquinone sulfonic acid (HQS)
5	1,4-dihydroxynaphthalene
6	anthraquinone-2-sulfonic acid
7	2-phenylhydroquinone
8	2,3-dihydroxypyridine
9	3,6-dihydroxypyridazine (maleic hydrazide)
10	2,5-dihydroxythiophenol (DHT)
11	2-octyl-1,4-benzenediol (DHOT)

CHAPTER III

RESULTS AND DISCUSSION

The Clean and Well-Characterized Electrode Surface

In this study, the compositional and structural integrity of the electrode surface was always determined prior to the chemisorption experiments. Such evaluation was based upon AES, LEED and HREELS.

Figure 21 shows the AES spectra of a clean Pd(111) surface. Pd consists of three peaks with kinetic energies at 239 eV, 275 eV and 326 eV. The standard kinetic-energies are 243 eV, 279 eV and 330 eV.[55] The 4-eV shift is due to the spectrometer work-functions difference. The purpose of using AES in our studies is to confirm the existence of elements on the crystal surfaces. Usually, accurate quantification of AES peaks is not desired. Thus to identify an element, the absolute peak position is not applied as criterion, instead, relative peak positions to that of metal substrate (Pd) is utilized to determine surface elemental composition. Some elements have characteristic pattern in the AES spectra. For example, Cs has two peaks at 563 eV and 575 eV with almost identical intensities. Other elements of interest in the present study are: S, K, C, O, and I. Their AES kinetic energies are highlighted in Figure 21 by dashed lines. Sulfur has the higher Auger yield factor (84.53), while carbon has the lower (18.76). Thus it is relatively easy to identify contamination from sulfur than that from other elements. The overlap of K and C with Pd substrate peaks complicates their detection. Distortion of the Pd peaks can be used as an indication of the presence of these two elements.

Figure 22 shows the LEED spot pattern for a clean and atomically smooth Pd(111 surface. The sharp and bright hexagonal spots suggest continuous and sufficiently large

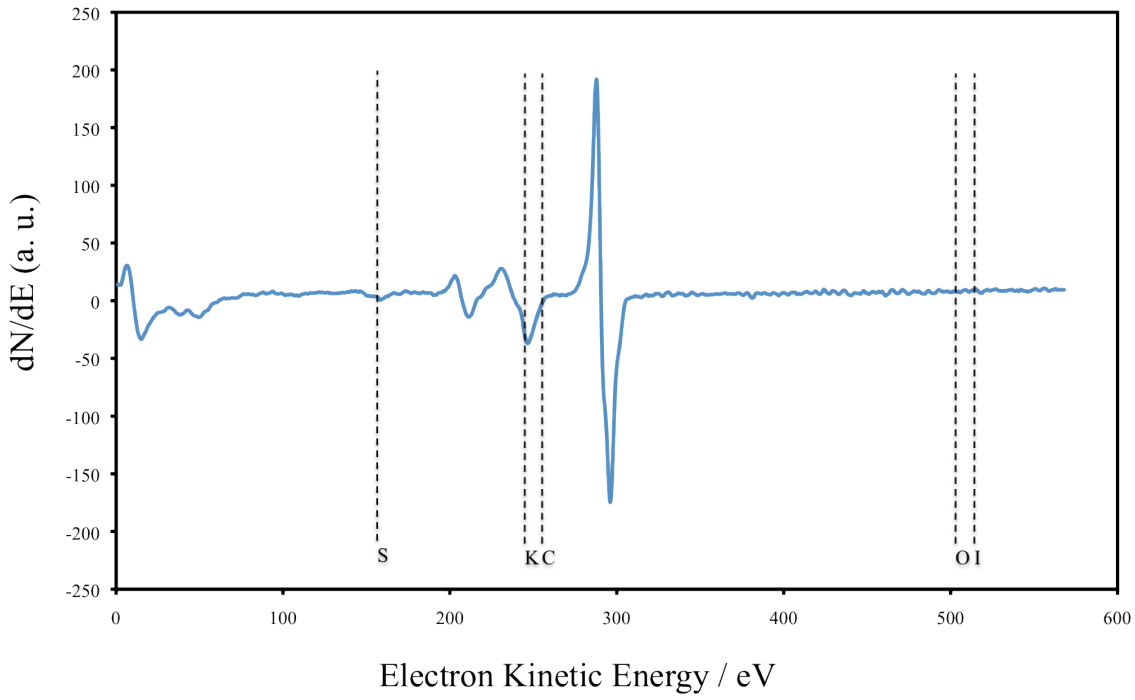

Figure 21. AES spectrum of a clean Pd(111) single crystal surface. Incident beam energy = 2 keV; beam current = 1 μA. The dashed lines represent the peak positions for species often encountered in this study.

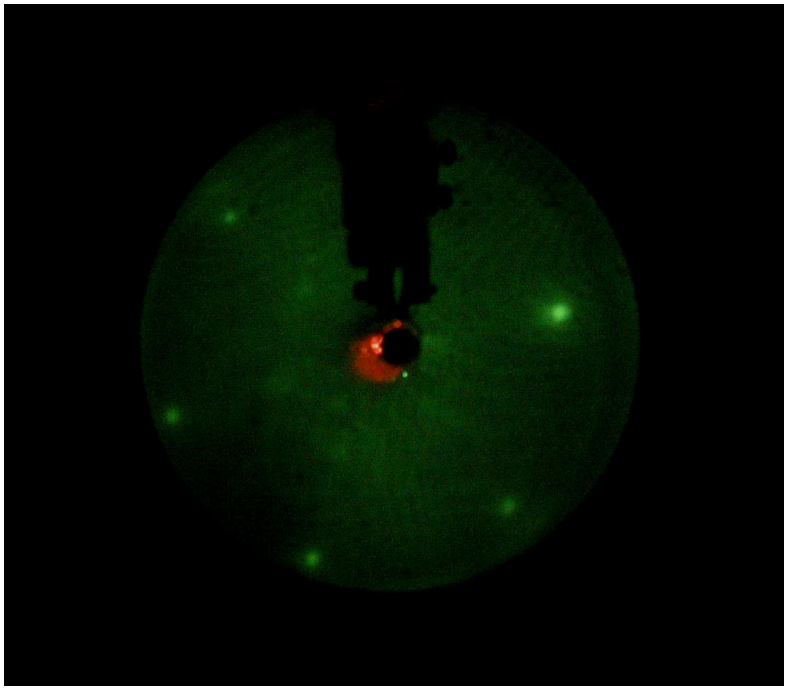

Figure 22. LEED pattern of a clean and well ordered Pd(111) single crystal surface.

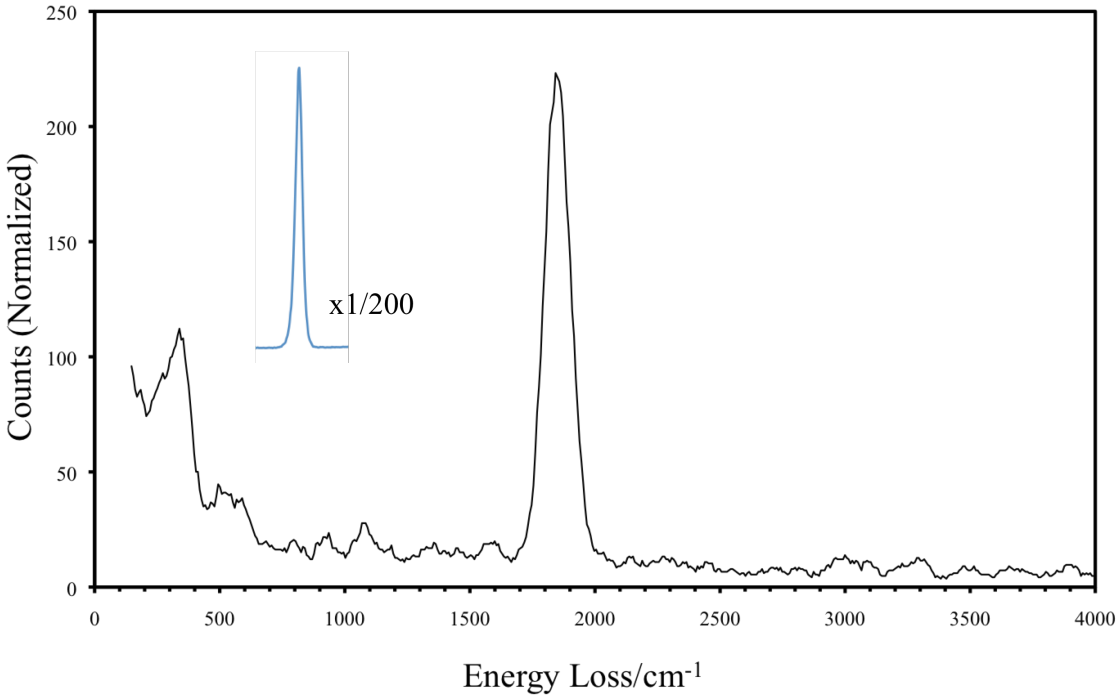

Figure 23. HREEL spectrum of a UHV-prepared Pd(111) surface with chemisorbed CO (<0.01 monolayer). Inserted is the attenuated elastic peak.

domains (>100Åx100Å) at the surface. In this study, however, LEED has not been used to determine the structure of the organic adlayers since that would have required intensity vs. voltage curves and subsequent LEED simulation computations. [56,57]

HREELS is oftentimes more sensitive than AES in the detection of molecular contaminants. Figure 23 shows a typical HREEL spectrum for a freshly prepared, well-ordered Pd(111) surface. The spectrum shows two peaks at 331 cm^{-1} and 1842 cm^{-1}, which can be assigned to ν(Pd-C) and ν(CO) modes respectively, as a result of the chemisorption of CO from the residual gas inside the UHV chamber. These data are in close agreement with reported data (325 cm^{-1}, 1820 cm^{-1} respectively),[58] It was reported also that, at low coverage, CO chemisorption occupies hollow sites (with frequency of 1828-1830 cm^{-1}) on (111) surfaces, while occupying bridge sites (1893 cm^{-1}) on (100) surfaces.[59-61]

Additional experiment showed that these CO peaks slowly increase their intensities within an hour immediately after the UHV preparation. Thermal annealing to 775 K was able to restore the CO-free Pd surface. The peak intensity for the ν(CO) stretching indicates only a small coverage (<0.01 monolayer), which explains the fact that such CO is not detectable by AES.

Hydroquinone Substituted with Methyl Groups

2,3-dimethylhydroquinone

HREELS spectra of chemisorbed 2,3-dimethylhydroquinone over a concentration range between 0.05 mM to 5 mM are shown in Figure 24. Identification of orientational changes based on the intensity ratio of γ(CH) and ν(CH) is beset with practical difficulties, for example, both the γ(CH) and ν(CH) are either very weak or show multiple

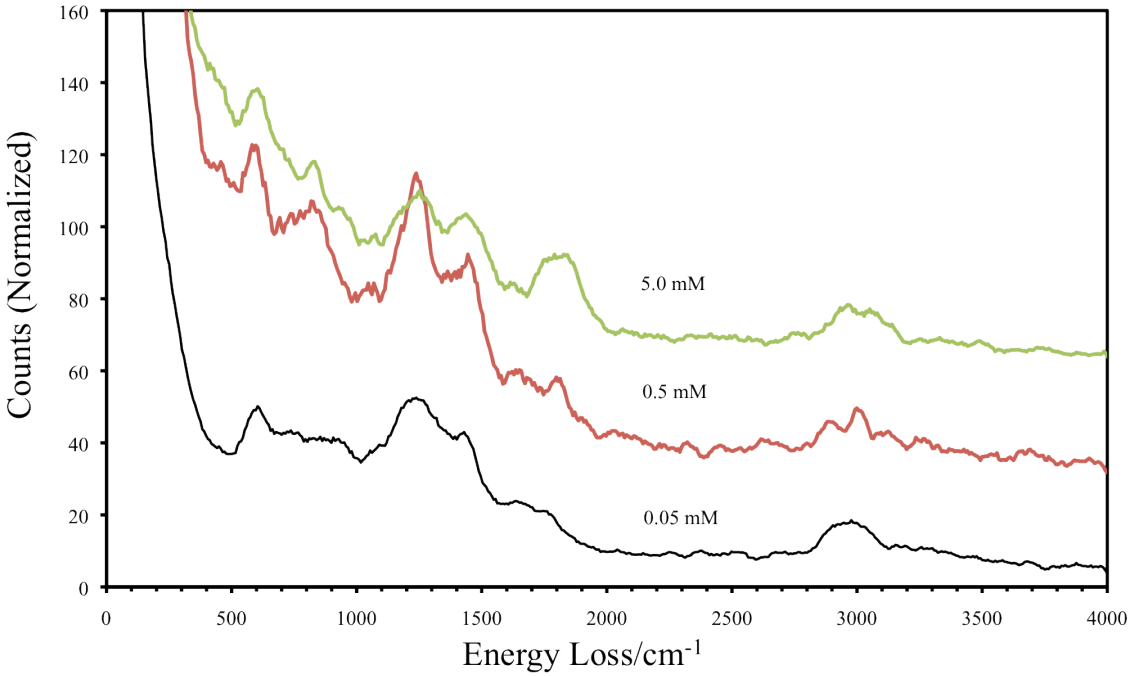

Figure 24. HREELS spectra of 2,3-dimethylhydroquinone chemisorbed on Pd(111) surfaces at the different concentrations.

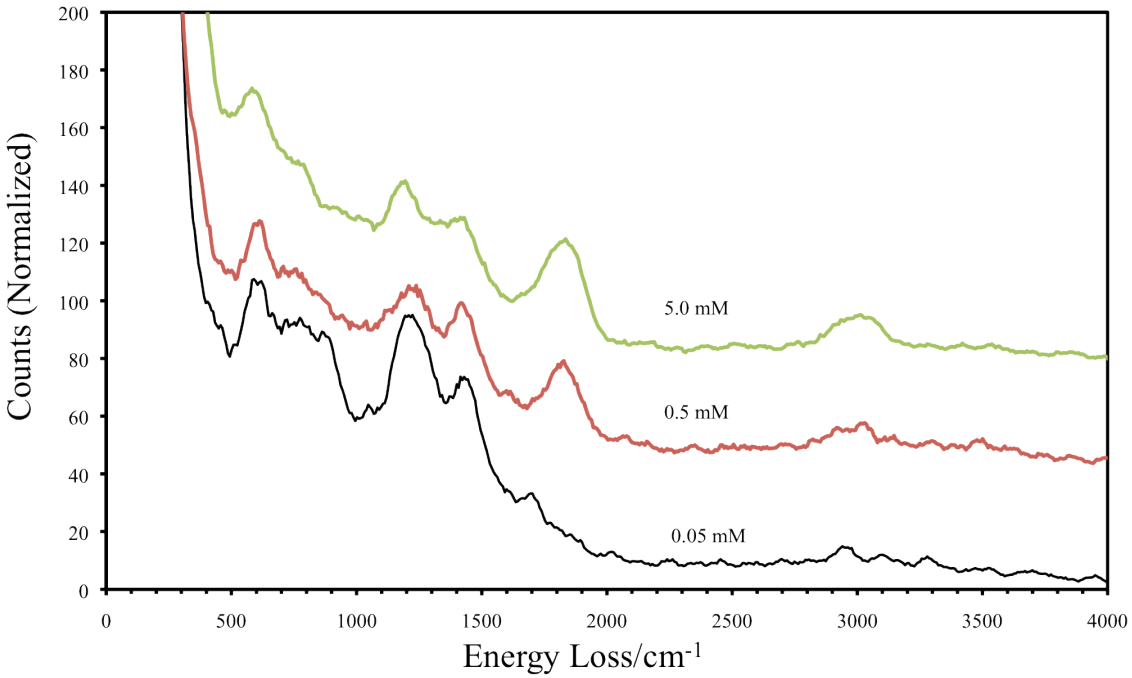

Figure 25. HREELS spectra of 2,3,5-trimethylhydroquinone chemisorbed on Pd(111) surfaces prepared from 0.05 mM, 0.5 mM and 5 mM solutions.

broad peaks. These unexpected spectral features are similar to those reported for similar compounds. As an example, HREELS work with o-xylene, which is just 2,3-dihydroxyhydroquinone without the hydroxy groups,[62] shared the same broad and multiple ν(CH) peaks.

2,3,5-trimethylhydroquinone

HREELS was also carried out with 2,3,5-trimethylhydroquinone. As can be seen in the spectrum in Figure 25, the broad and multiple peaks of ν(CH) are essentially identical to that of 2,3- diphenolichydroquinone. It is not understood at this time why the ν(CH) peaks are drastically dependent upon the addition of the methyl substituents. The possibility exists that the C-H stretching of the CH_3 group overlaps with the ν(CH) peak of the aromatic ring.

Further studies with complementary techniques such as EC-STM and IR reflection absorption spectroscopy (which has higher resolution than HREELS) will be necessary.

Hydroquinone Substituted with a Sulfonate Group

Benzoquinone sulfonic acid (BQS) chemisorbed from low concentration (0.1mM) on Pd(111) has been studied by EC-STM.[63] Figure 26 shows the image of a 3×3 adlayer of chemisorbed BQS. A surface corrugation study revealed a tilted diphenolic ring with respect to the Pd(111) surface. This is not unexpected since the sulfonate group is rather bulky and would sterically hinder a rigidly flat orientation. No visible counter cations were observed, which is anticipated since they are non-chemisorbed and would be quickly displaced from their initial locations by the STM tip. The proposed geometry of chemisorbed BQS on Pd(111) is shown in Figure 27.

Figure 28 shows the DFT-optimized structure of BQS in the flat orientation on Pd(111) surface. It can be seen that: (a) The quinone moiety is no longer completely planar. (b) the C-H bonds are slightly tilted away from the ring plane. This may help explain the HREELS-activity of the in-plane C-H stretching. (c) The top layers of Pd(111) are slightly distorted permanently to maximize d-orbital overlap with the π-system of the HQS molecule. Whether or not chemical or physical adsorption is occurring can be predicted by the total energy change (adsorption energy). If adsorption energy is less than 0.3 eV, it is generally considered physisorption, while a typical chemisorption yields adsorption energy more than 1 eV.[64] Fine calculation of the adsorption energy of Pd(111)-η^6-HQS yielded 2.41 eV, indicating a chemisorption.[65]

Figure 29 shows the HREELS spectra of chemisorbed BQS on Pd(111) prepared from 0.05 mM, 0.5 mM and 5.0 mM solutions.

It was reported that the region between 500 cm^{-1} to 1500 cm^{-1} is obscured by sulfuric acid supporting electrolyte. This shroud effect could be reduced by rinsing the Pd(111) surfaces with deionized water.[19]

Further investigation was carried out with adsorbate-covered Pd(111) surfaces. Figure 30 shows HREELS spectra of chemisorbed 3,6-dihydroxypyridazine prepared in 0.05 mM solution concentration, and consecutively rinsed with pH 7 buffer. It can be seen that: (a) C-H out-of-plane bending peak (840 cm^{-1}) recovered its flat baseline. (b) Previously sharp peak at 582 cm^{-1} (O-S-O bending) diminished to a broad, less symmetrical peak. (c) There is no frequency shift for either C-H out-of-plane bending mode or C-H stretching mode (3058 cm^{-1}). (d) The intensities of both C-H out-of-plane bending and C-H stretching increased after rinse, indicating reduced shroud effect from

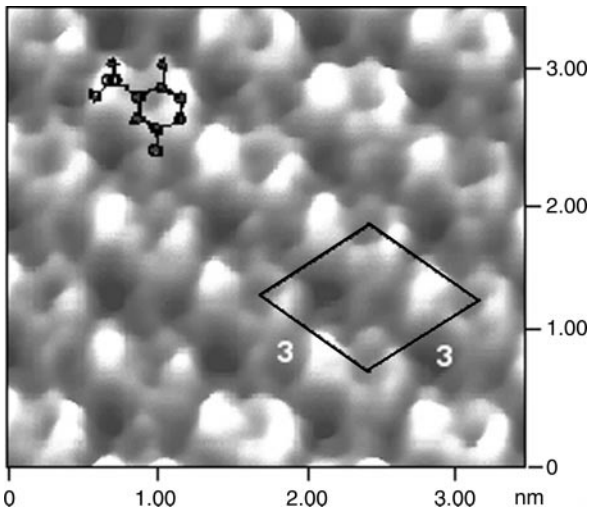

Figure 26. STM image of 3×3 adlayer of hydroquinone sulfonic acid chemisorbed on Pd(111) surface. Bias voltage: 100 mV; tunneling current: 30 nA.

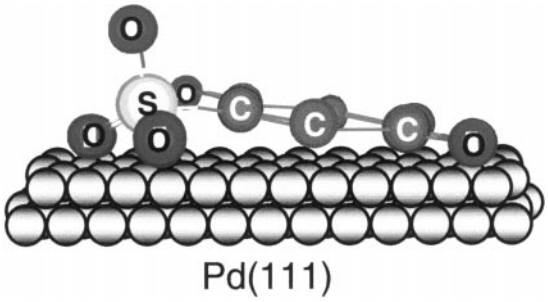

Figure 27. Molecular model of BQS chemisorbed on Pd(111) in the tilted-flat orientation.

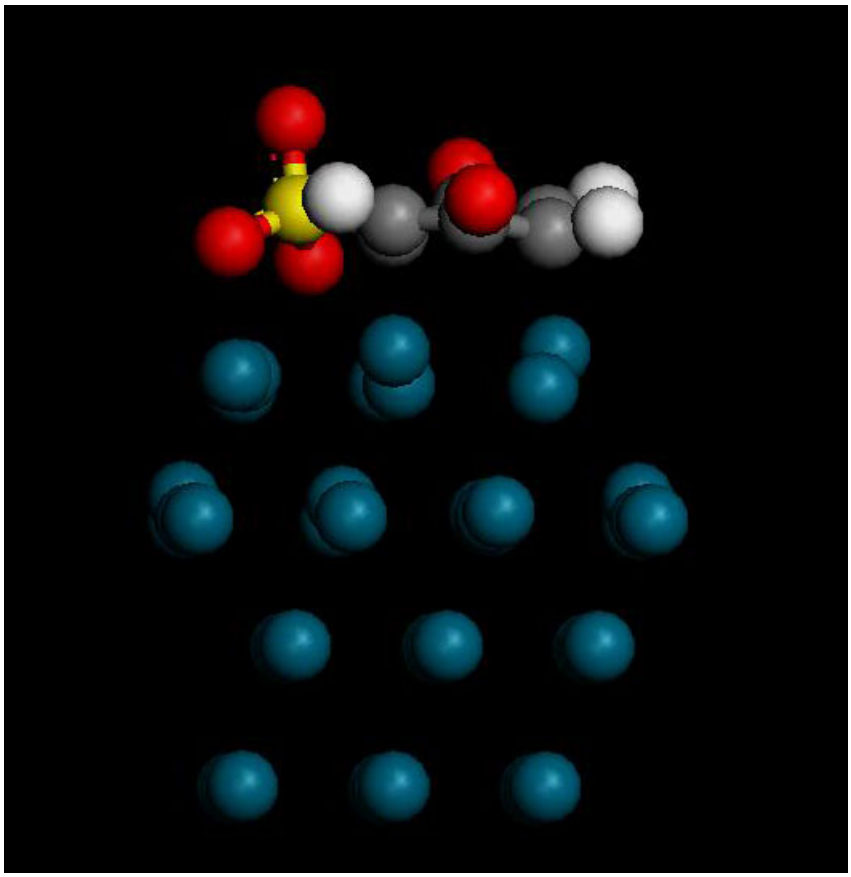

Figure 28. DFT optimized structure of chemisorbed BQS in the flat orientation on Pd(111).

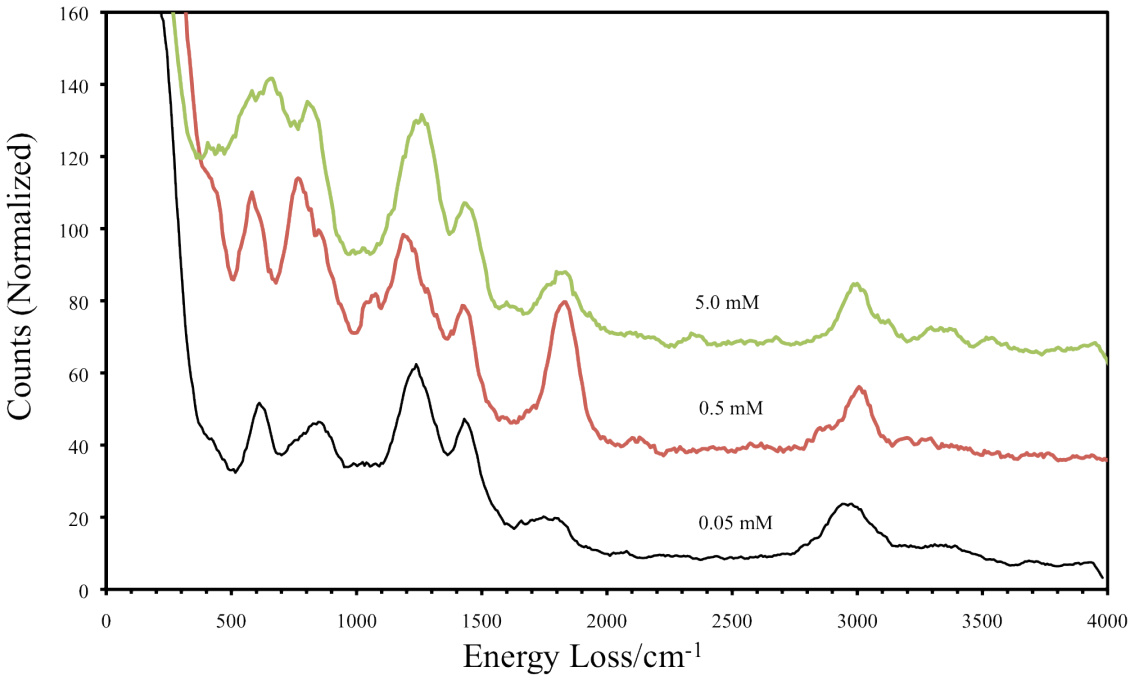

Figure 29. HREELS spectra of BQS chemisorbed on Pd(111) surfaces prepared from 0.05 mM, 0.5 mM and 5.0 mM solutions.

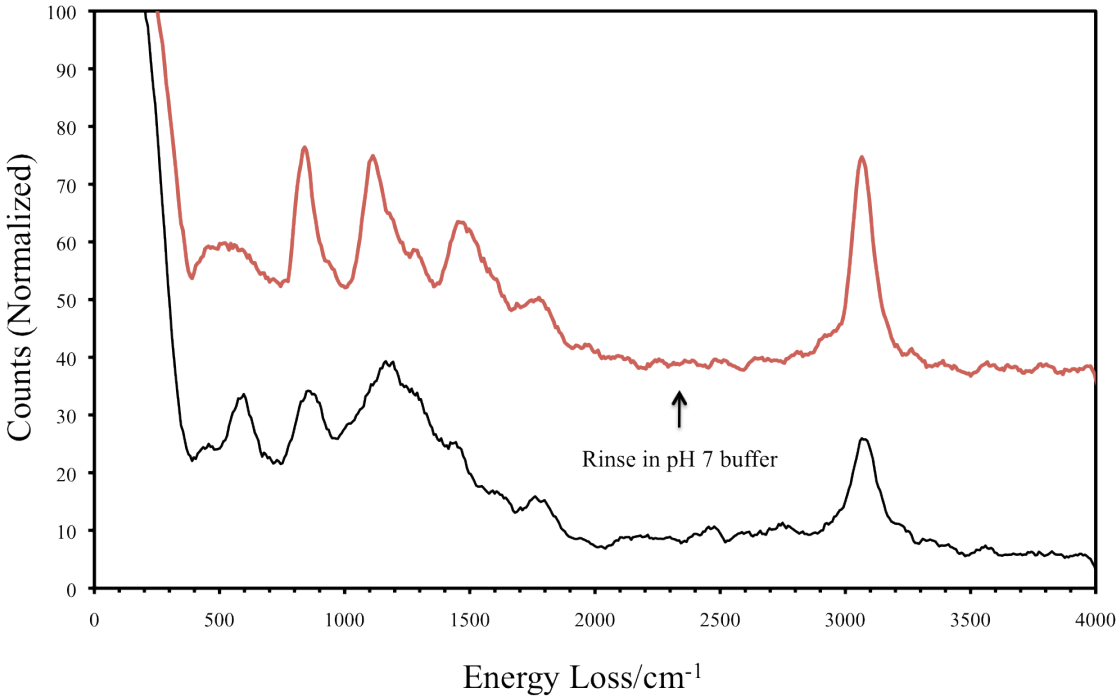

Figure 30. HREELS spectra of chemisorbed 1,4-paridazinedione before and after a rinse in pH 7 buffer.

H_2SO_4, although their peak intensity ratios before and after the rinse remains similar. STM studies reveals that when Pd(111) surfaces are exposed to sulfuric acid, coordinative chemisorption (Pd-O-SO_3H) is formed and possibly dissociated into the ionic form.[66] Conclusions based on the analysis above can be drawn as: (a) Even under UHV, H_2SO_4 is still present on the surface (in dissociated form). (b) The consecutive rinse with pH 7 buffer (containing HCO_3^- and SO_4^{2-}) was able to remove, at least partially residual H_2SO_4, possibly in the dissociated form (SO_4^{-2} or HSO_4^-), (c) The chemisorbed 3,6-dihydroxypyridazine strongly bind to Pd surface and is a stronger ligand than SO_4^{-2} (or HSO_4^-). (d) Residual H_2SO_4 bind to surface at the vacancies between the 3,6-dihydroxypyridazine molecules.

The H_2SO_4, despite its shroud effect, is still used as the supporting electrolyte in the present study to minimize contamination and to provide sufficient conductivity.[19]

For the these reasons discussed above, the region between 500 cm^{-1} to 1500 cm^{-1} is obscured by peaks due to coadsorbed electrolyte anions (sulfate/bisulfate) at the higher concentrations studied. Therefore only the spectra at 0.05 mM and 0.5 mM are discussed here. The intensity ratio γ(CH)/ν(CH) increases from 0.68 at 0.05 mM to 2.74 at 0.5 mM. This dramatic change indicates a transition from the flat orientation to an edgewise orientation.

It may be additionally noted that: At the concentration of 0.05 mM, the C-H stretching peak is rather broad (centered at 2947 cm^{-1}). At higher concentrations, this peak is narrowed and shifted higher frequencies (2992cm^{-1} for 0.5 mM; 2984 cm^{-1} for 5.0 mM). The rationales for these changes are not well-understood. They are undoubtedly due to either adsorbate-adsorbate interactions and/or orientational change.

Hydroquinone Fused with Aromatic Rings

1,4-dihydroxynaphthalene

Figure 31 shows the HREELS spectra of 1,4-naphthalenedione chemisorbed on Pd(111) surfaces prepared from 0.05 mM, and 2.0 mM solutions. The γ(CH)/ν(CH) intensity ratios are 1.42 for 0.05 mM and 1.35 for 2 mM. The fact that these intensity ratios are essentially constant indicates the absence of a change in orientation, at least within this concentration range.

Anthraquinone-2-sulfonic Acid

Figure 32 shows the HREELS spectra of anthraquinone-2-sulfonic acid chemisorbed on Pd(111) surfaces from 0.05 mM, and 5.0 mM solutions. γ(CH) is obscured by the existence of a broad and intense peak at 604 cm^{-1} (O-S-O bending). However, based on previous TLE studies on polycrystalline platinum, it can be postulated that this compound adopts a flat orientation within this concentration range.[22] This resistance to reorientation is probably facilitated by both energetic and entropic effects: at flat orientation, all three rings can interact more strongly with the metal surface and displace more water molecules relative to the edgewise.

Hydroquinone Substituted with a Phenyl Group

2-phenylhydroquinone is studied as the model diphenolic molecule with a non-fused phenyl substituent. The flexibility of the phenyl group, relative to anthraquinone and naphthalene, may render it unusual chemisorption properties. Previous studies with 2-phenylhydroquinone on polycrystalline platinum revealed three orientational transitions: (a) at concentrations lower than 0.1 mM, the benzoquinone moiety and phenyl ring were both bonded to platinum in a flat orientation; (b) at concentrations

between 0.1 mM and 1 mM, both groups reoriented to an edgewise configuration; (c) at still higher concentrations (> 1 mM), an increased packing density resulted in the benzoquinone moiety was chemisorbed edgewise but the phenyl ring was now pendant.[22]

Figure 33 shows HREELS spectra of 2-phenylhydroquinone chemisorbed on Pd (111) surfaces from 0.05 mM, 0.5 mM and 5.0 mM solutions. Because of ill-understood complications, the γ(CH)/ν(CH) intensity ratio could not be used as a criterion to ascertain changes in orientation. However, a closer look at the spectra reveals some relevant information: at 0.05 mM, ν(CH) shows a single peak at 2862 cm^{-1}; as the concentration is increased to 0.5 mM, ν(CH) is split into two peaks at 2910 cm^{-1} and 3014 cm^{-1}, with the former being twice intense than the latter; at 5.0 mM, the relative intensities of these two peaks converge to the same value. This vibrational finger print is in consonance with the orientation transition postulated in the case of 2-phenylhydroquinone chemisorption on platinum.

Further information with respect to chemisorption properties of 2-phenylhydroquinone may be explored by cyclic voltammetry since, if the diphenolic ring is pendant, its electrochemical activity (Q/H_2Q redox) should be preserved. Figure 34 shows the cyclic voltammograms of 2-phenylbenzoquinone (PBQ) and 2-(8-mercaptooctyl)-1,4-Benzenedione (DHOT) at similar surface packing densities (Γ_{DHOT} = 0.54 $nmolcm^{-2}$; Γ_{PBQ} = 0.46 $nmolcm^{-2}$). As discussed further below, chemisorbed DHOT displays a quasi-reversible redox peak at 0.36 V since the binding is through the alkane thiol with the hydroquinone moiety unadsorbed. On the other hand, the chemisorbed 2-phenylbenzoquinone does not show any redox activity. This can only be understood if it

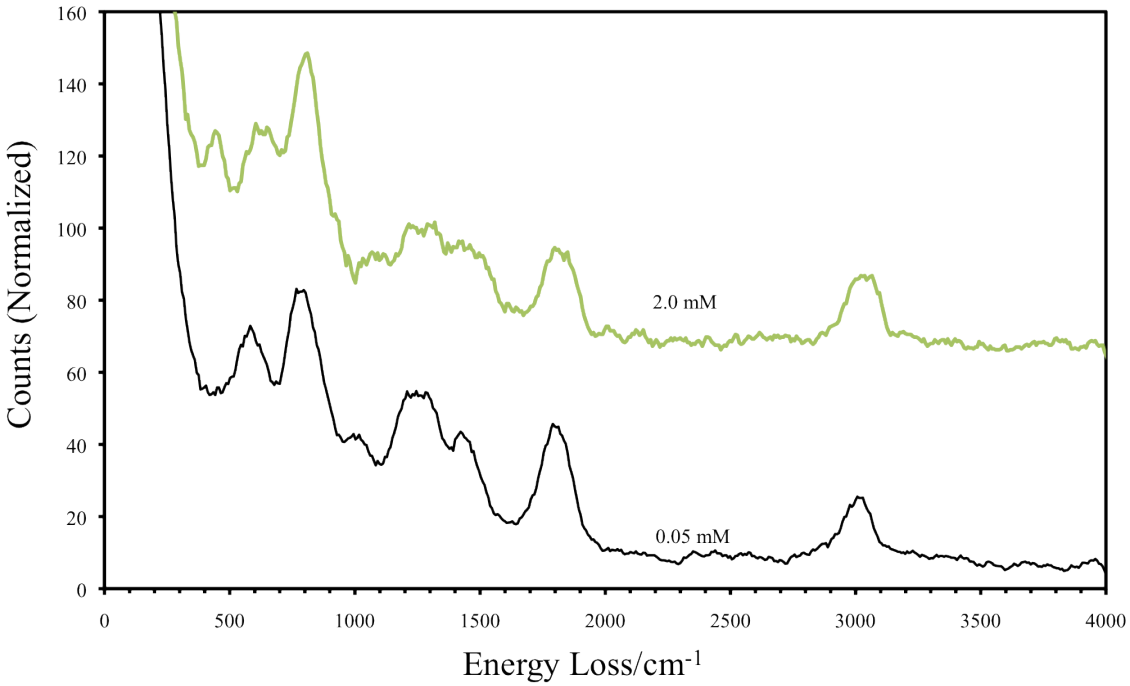

Figure 31. HREELS spectra of 1,4-dihydroxynaphthalene chemisorbed on Pd(111) surfaces prepared from 0.05 mM, and 2.0 mM solutions.

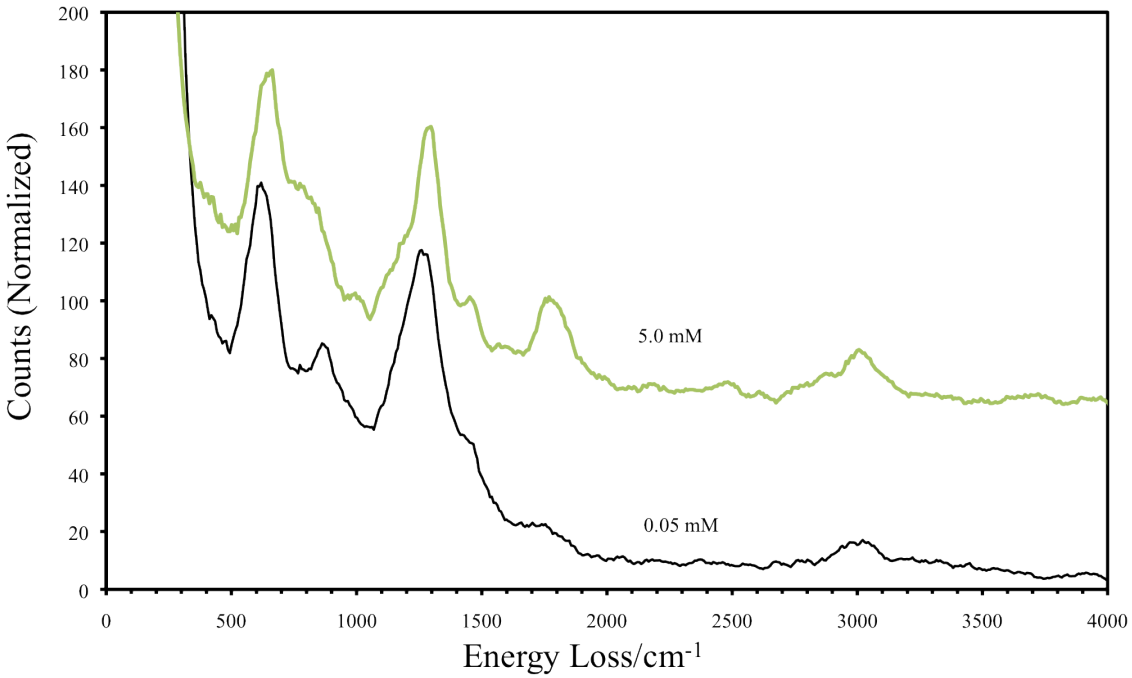

Figure 32. HREELS spectra of anthraquinone-2-sulfonic acid chemisorbed on Pd(111) surfaces prepared from 0.05 mM, and 5.0 mM solutions.

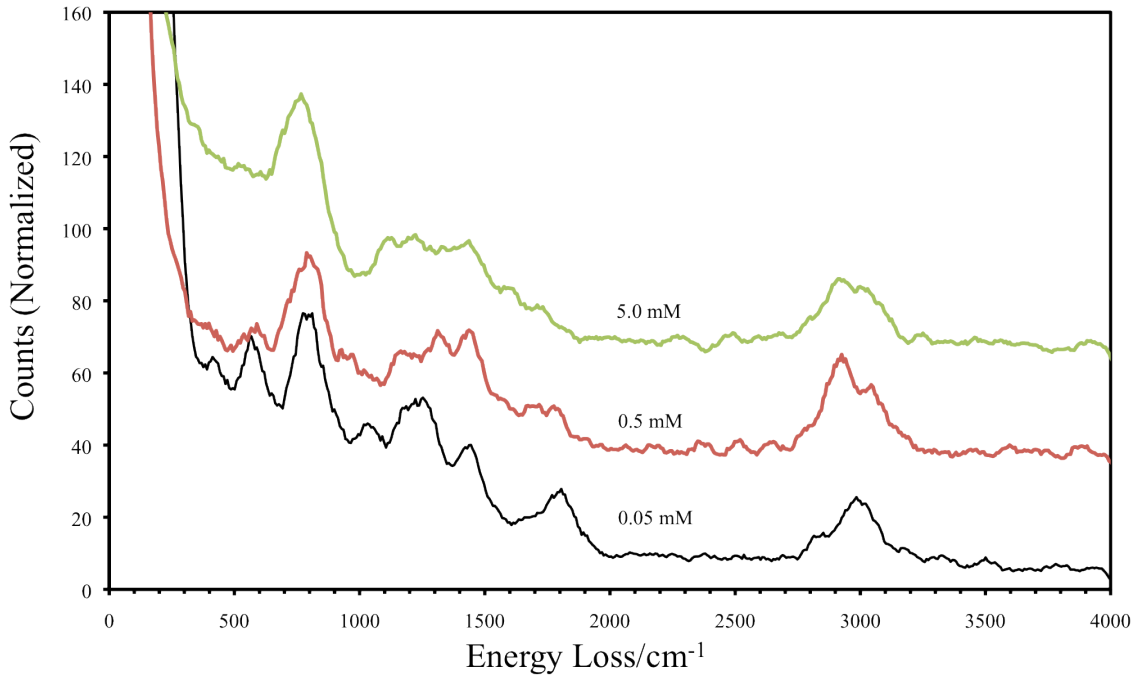

Figure 33. HREELS spectra of 2-phenylbenzoquinone chemisorbed on Pd (111) surfaces prepared from 0.05 mM, 0.5 mM and 5.0 mM* solutions.

*approaching solubility limit

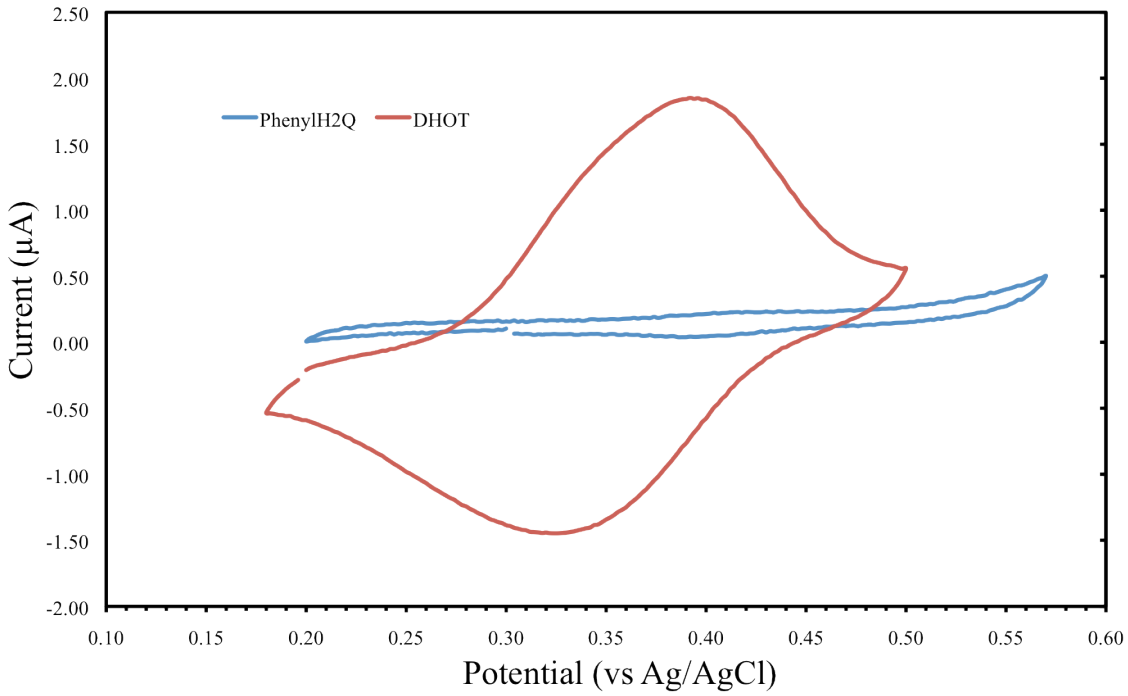

Figure 34. Cyclic voltammograms of chemisorbed 2-phenylhydroquinone and 2-(8-mercaptooctyl)-1,4-benzenedione with similar coverages.

is assumed that the hydroquinone moiety is chemisorbed (as the quinone), which renders it electrochemically inert. Therefore, it is the phenyl ring that is pendant.

This postulated chemisorption configuration is further supported by other studies that compare the strength of chemisorption of BQ and benzene.[67] In anodic oxidation and cathodic hydrogenation experiments via differential electrochemical mass spectrometry (DEMS), it was found that benzene was desorbed (not reacted electrocatalytically) near the hydrogen-evolution region and at the onset of oxygen adsorption region. In contrast, benzoquinone was oxidized and hydrogenated. These results strongly suggest a much weaker binding of benzene moiety to BQ on Pd surfaces.

N-heteroatomic Diphenols

The N-heteroaromatic molecules introduce the possibility that the N-substrate interactions will strongly influence the chemisorbed molecule orientation.

2,3-Dihydroxypyridine and 3,6-dihydroxypyridazine have been studied on polycrystalline Pt surfaces.[21,22] It was reported that: (a) the N-heteroatom is more strongly surface active than the π-system of the aromatic ring, and (b) the mode of chemisorption of the pyridine derivative is substantially pH-dependant because of the appreciable basicity of the N heteroatom. In this work, the effect of pH on the chemisorption of the selected compounds on Pd was also explored (at pH 2 and pH 7). More basic solutions were not studied due to the fact that the hydroxyl ion is moderately surface active on Pd and would considerably interfere with the chemisorption of the N-heteroaromatic compounds.

2,3-dihydroxypyridine

The acid dissociation constant of 2,3-dihydroxypyridine is documented as pK_a = 8.12 for the protonated N heteroatom.[68] At pH 2, complete protonation of nitrogen heteroatoms is expected, while at pH 7, small portions (~10%) of nitrogen heteroatoms will be in basic form. The HREELS spectra of 2,3-dihydroxypyridine chemisorbed on Pd(111) prepared from pH 2 and pH 7 solutions are shown in Figures 35 and 36 respectively. The intensity ratio of γ(CH)/ν(CH) is 0.94 at pH 2 but three-fold lower at pH 7. The C-H stretching mode is more prominent at pH 7 than at pH 2, while the opposite trend is shown in the N-H stretching mode (~3300 cm^{-1}). These clearly point to changes in the adsorbed-molecule orientation.

The results indicate that, at pH 2, the N-heteroatom is initially protonated in solution, which serves to facilitate the chemisorption via the π-system and enforce a flat orientation. At pH 7, the degree of protonation is much less severe; hence, chemisorption is predominantly through the N lone pair that leads to an endwise (N-η^1) orientation.

3,6-dihydroxypyridazine

The HREEL spectra for 3,6-dihydroxypyridazine at pH 2 and pH 7 chemisorbed from different concentrations are shown in Figures 37 and 38, respectively. Compared to the previous pyridine derivative, the acid dissociation constant of 2,3-dihydroxypyridine is significantly lower (pK_{a1} = 2.60).[68] No N-H stretching mode was observed for the chemisorbed compounds from either pH 2 or pH 7. At pH 7, the γ(CH)/ν(CH) intensity ratio remains essentially unchanged over the concentration range studied. At pH 2, on the other hand, the γ(CH)/ν(CH) intensity ratio decreased as the solution concentration

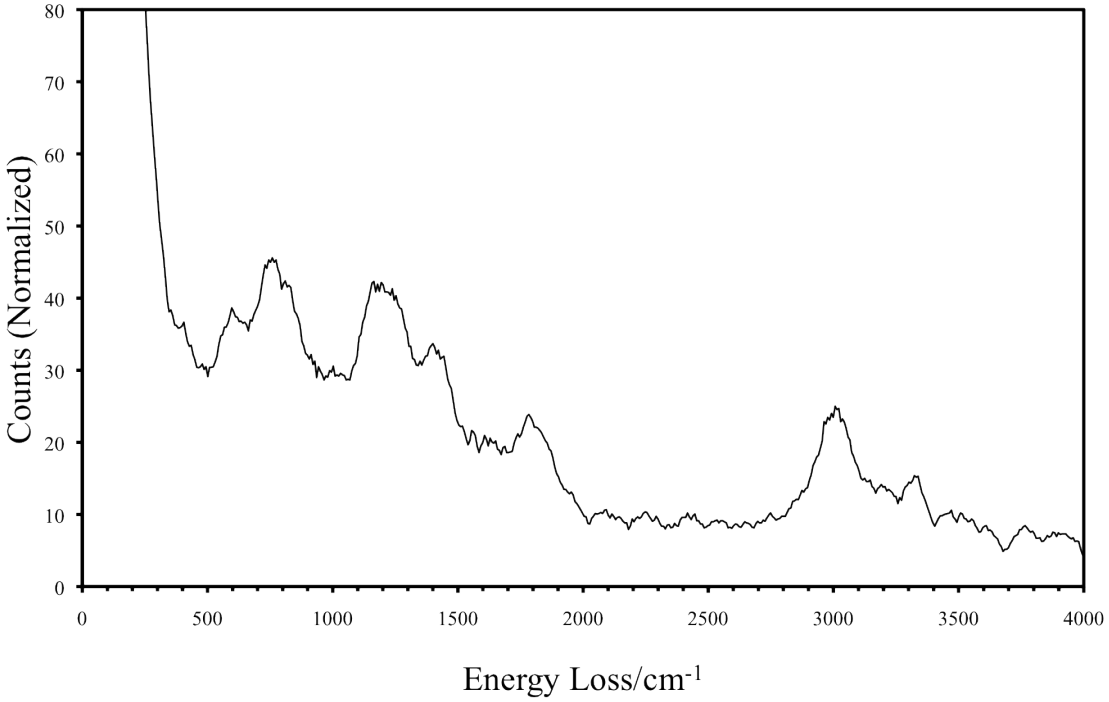

Figure 35. HREEL spectrum of 2,3-Dihydroxypyridine chemisorbed on Pd(111) surface from 0.05 mM solution at pH 2.

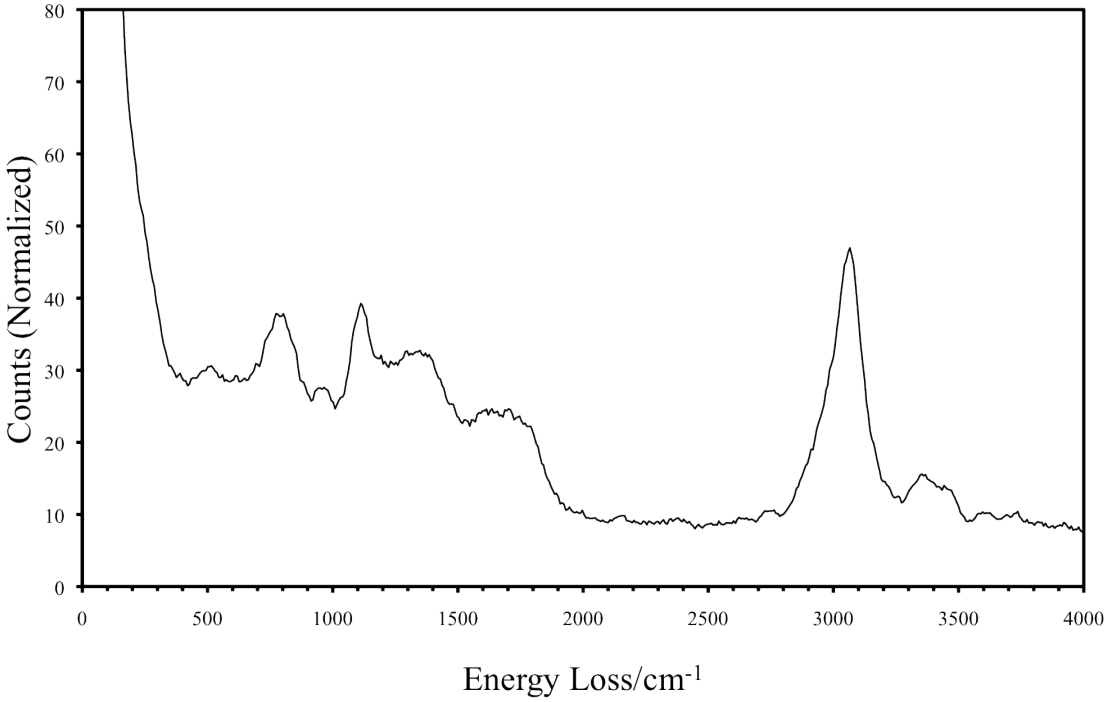

Figure 36. HREEL spectrum of 2,3-Dihydroxypyridine chemisorbed on Pd(111) surface from 0.05 mM solution at pH 7.

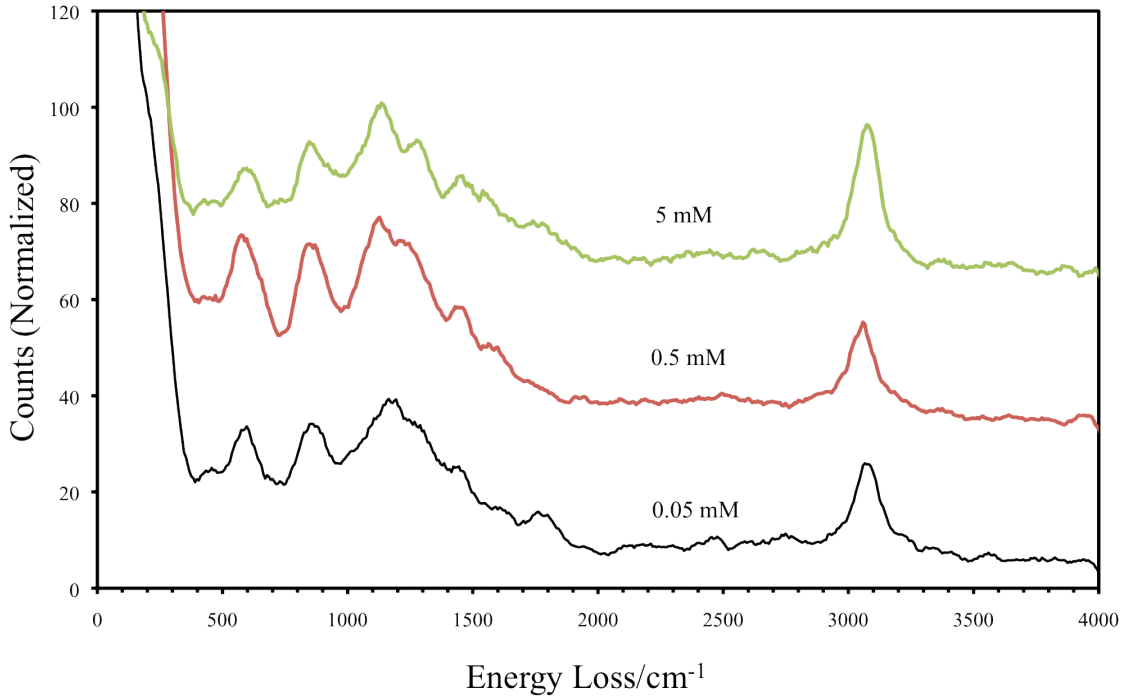

Figure 37. HREELS spectra of 3,6-dihydroxypyridazine chemisorbed on Pd(111) surface from 0.05 mM, 0.5 mM and 5 mM solutions at pH 2.

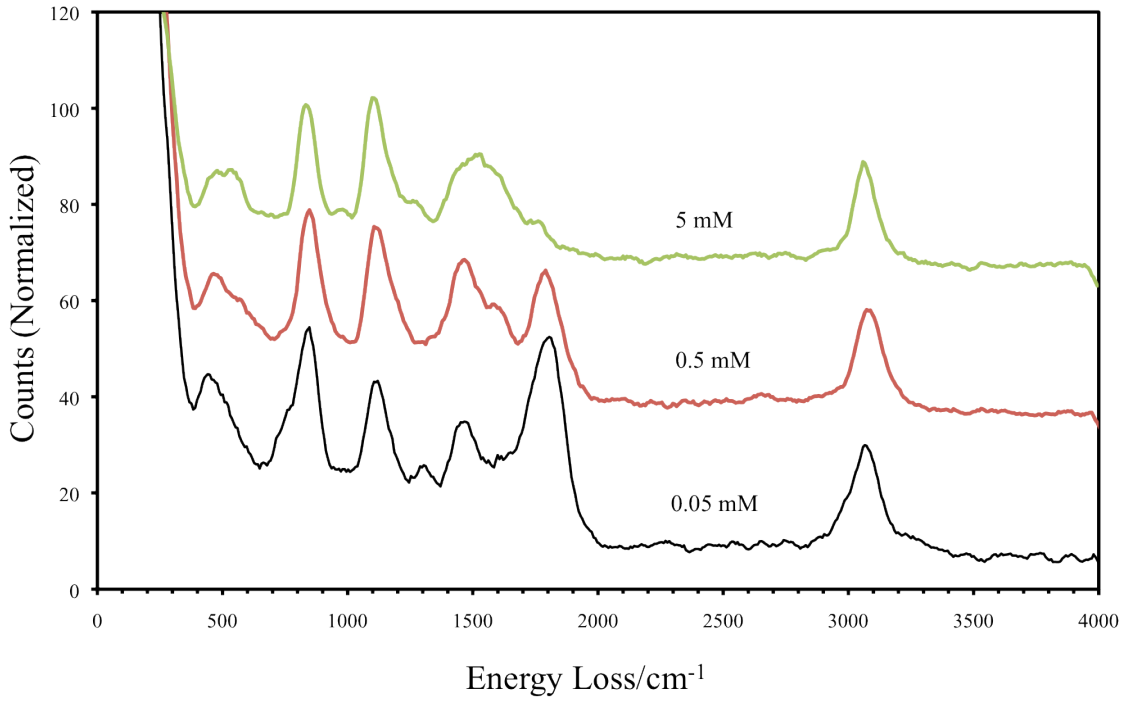

Figure 38. HREELS spectra of 3,6-dihydroxypyridazine chemisorbed on Pd(111) surface prepared from 0.05 mM, 0.5 mM and 5 mM solutions at pH 7.

increased. This can only happen if the molecules were adsorbed via the N lone pair, in this case, the C-H stretching mode would be much more prominent.

The results further indicate that, at pH 2, the N-heteroatom is partially protonated in solution, which allows the π-system of aromatic ring to be competitively surface active. At pH 7, the degree of protonation is much lower; hence, chemisorption is predominantly through the N lone pair that leads to an endwise (N-η^1), perhaps fluxional orientation.[22]

Hydroquinone Substituted with Mercapto Groups

This type of substituted diphenol are represented by 2,5-dihydroxythiophenol (DHT) and 2-(8-mercaptooctyl)-1,4-Benzenediol (DHOT).

Figure 39a shows the positive potential cycle of cyclic voltammogram of DHT chemisorbed from 0.02 mM solution. There is no discernable anodic current from the H_2Q-to-Q redox reaction. Previous studies at the polycrystalline electrodes revealed that, when DHT is chemisorbed at low coverages on Au, the Q/H_2Q redox chemistry is preserved; this indicates that, on this metal, the diphenolic moiety remains fully pendant. However, when DHT was chemisorbed at low coverages on Pt, no redox activity was observed.[69] Such loss of activity was rationalized to be due to the chemisorption of the diphenolic ring, in addition to that of the –SH group. Hence, at very low coverages, both the -SH and diphenolic groups simultaneously bind to the Pt surface in a chelation reaction. Similar results were obtained for Ir and the expectation was that identical surface chelation chemistry would also transpire at Pd electrode.[70,71]

This scenario was further explored via coadsorption studies with iodine. It was earlier found that I^- is much more surface active than the diphenolic ring.[57,72,73] Hence,

exposure of the surface that contained the chelated DHT molecule to a dilute solution of KI would result in the displacement of the aromatic ring from the surface due to the oxidative ($I^-_{(aq)}$-to-$I_{(ads)}$) chemisorption of iodine. The then pendant diphenolic moiety would exhibit its reversible quinone-to-diphenol redox activity. This expectation is borne out by the results in Figure 39b. The voltammetric features are quite similar to those obtained when identical experiments were performed on polycrystalline Pt.[69]

When DHT is chemisorbed from a much higher concentrations, it is anticipated that the chemisorption driving force would favor exclusive surface attachment via the mercapto group. In this instance, since the diphenolic ring is pendant, reversible quinone-to-diphenolic redox activity would be exhibited. The result, in terms of a cyclic voltammogram of DHT chemisorbed from 5 mM solution, is shown in Figure 40. It is obvious that co-adsorption of I^- does not alter the redox activity as was the case for DHT chemisorbed from 0.02 mM solution.

It is important to recall earlier voltammetric experiments of DHT chemisorbed on Au and Pt. It was found that the redox peaks are abnormally broad for DHT on Pt but not abnormal on Au.[69,71,73] It was further found out that: (a) The peak broadening is induced by attractive interactions between adsorbed molecules.[74,75] (b) Such attractive forces are similar to those in the quinhydrone (1:1 Q:H_2Q) complex and favor the formation of a 1:1 Q-to-H_2Q ratio within the chemisorbed DHT layer. Face-to-face Q-to-H_2Q interactions have also been observed for non-chemisorbed species (on I coated Pd) by EC-STM.[76] (c) The full width at half maximum (FWHM) of DHT on Pt (0.21 V) is much bigger than that on Au (0.13 V), due to a stronger affinity of diphenolic moiety to Pt surface relative to Au surface. (d) When a -CH_2- group, which does not possess delocalized electrons, is

inserted between the diphenolic ring and the –SH group, as in the case of 2,5-dihydroxy-4-methylbenzenemercaptan (DHBM), the peak broadening effect disappeared on Pt.[69,71,77-79] Based on these results, it was postulated that the adsorbate-adsorbate interaction that led to redox peak broadening occurred through the substrate, but not through space; no such substrate-mediated interaction occurred on Au because the aromatic ring is inert toward it.

As an extension to the DHT studies, DHOT was also investigated. Recall, as already alluded to, insertion of a non-π-system like $–CH_2-$ between the –SH and diphenolic group severed the substrate-mediated adsorbate-adsorbate interactions on Pt, the existence of an 8-carbon alkyl chain on DHOT is expected to disrupt the $Q\text{-}H_2Q$ interactions that occurred through the Pd surface. That is, no broadening should be observed. Figure 41 provides voltammetric data that support this scenario: the voltammetric FWHM of chemisorbed DHT has decreased substantially from 0.19 V to 0.13 V. In addition, the redox reaction of the diphenolic moiety remains unchanged after co-adsorption of I.

HREELS experiments with chemisorbed DHT and DHOT were also carried out. The results are shown in Figures 42 and 43; peak assignments are listed in Table 2.[58,80] Pd-S-η^7-H_2Q represents DHT chemisorbed on a Pd surface as a chelate (0.02 mM). Pd-S-η^1-H_2Q denotes s-bonded DHT (5.0 mM), with the H_2Q group pendant.

There are a few points worth noting: (a) There is no observable S-H stretching peak at about 2500 cm^{-1}. This implies that, upon chemisorption, the S-H bond is activated due to the formation of a Pd-S bond. (b) The γ(CH)/ν(CH) intensity ratios are 0.97 for Pd-S-η^7-H_2Q and 1.41 for Pd-S-η^1-H_2Q. This significant change confirms that the

diphenolic ring adopts different orientations when chemisorbed on Pd surface at low and high concentrations. (c) The preservation of γ(CH) and ν(CH) from the aromatic ring indicates the aromatic ring remained intact upon chemisorption.

The HREEL spectrum of chemisorbed DHOT on from 0.04 mM solution is shown in Figure 44. Two major differences from Figure 43 are worth noting: (a) two C-H stretching peak at ~ 3000 cm^{-1}, and (b) less well-defined C-H bending peak at ~ 800 cm^{-1}. Based on a Lorentzian function fitting routine, two peaks at 2905 cm^{-1} and 3048 cm^{-1} are extracted for the C-H stretching peaks. These two peaks are assignable to alkyl -CH_2- and aromatic C-H stretching.[81,82] The intensity ratio of I_{2905}/I_{3048} was found to be 1.06. The close-to-unity ratio may be due to the fact that DHOT molecules are densely packed on Pd(111) surfaces so that only a small portion of -CH_2- is not shielded from the incident electrons. The broadened C-H bending peaks at ~ 800 cm^{-1} can be attributed to complications due to sterical hindrance within the closely packed adlayer. The diphenolic C-H stretching peak for DHT (5 mM DHT) and for DHOT are essentially identical (3043 cm^{-1} and 3048 cm^{-1}). This, of course, is expected since in both cases the diphenolic ring is pendant.

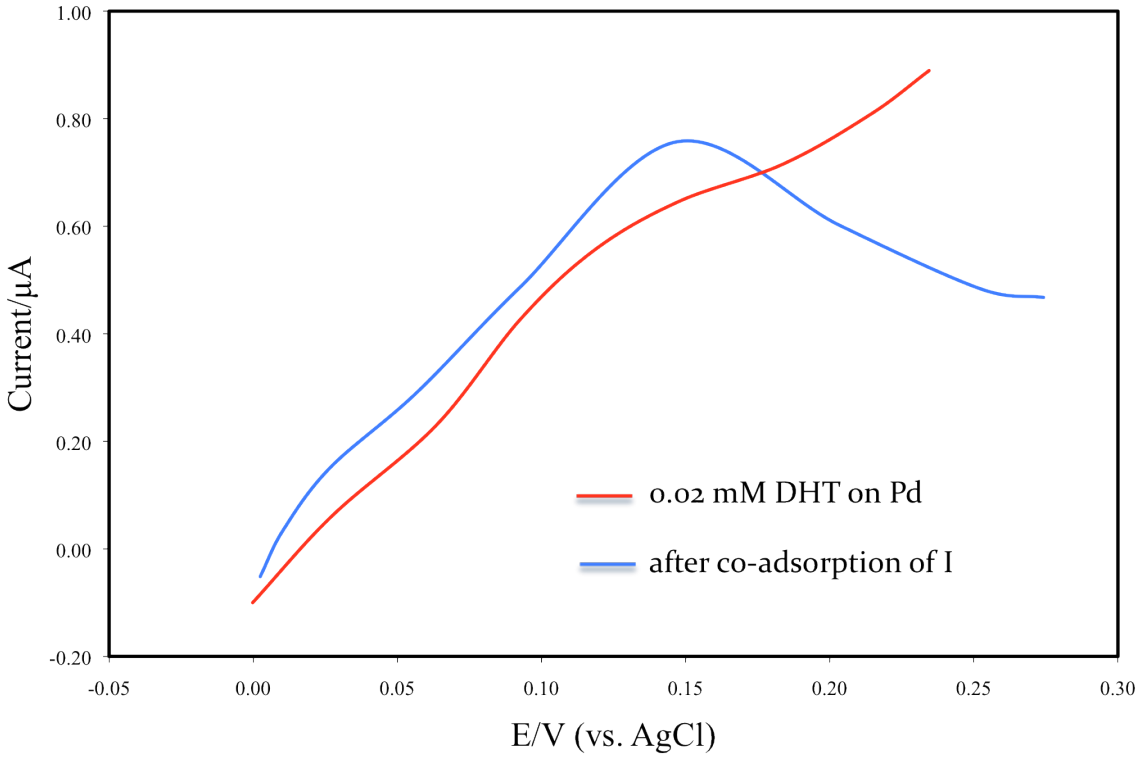

Figure 39. Positive potential cycle of cyclic voltammograms of DHT chemisorbed on Pd(111) surface prepared from 0.02 mM solution (a) before (red) and (b) after (blue) co-adsorption of I.

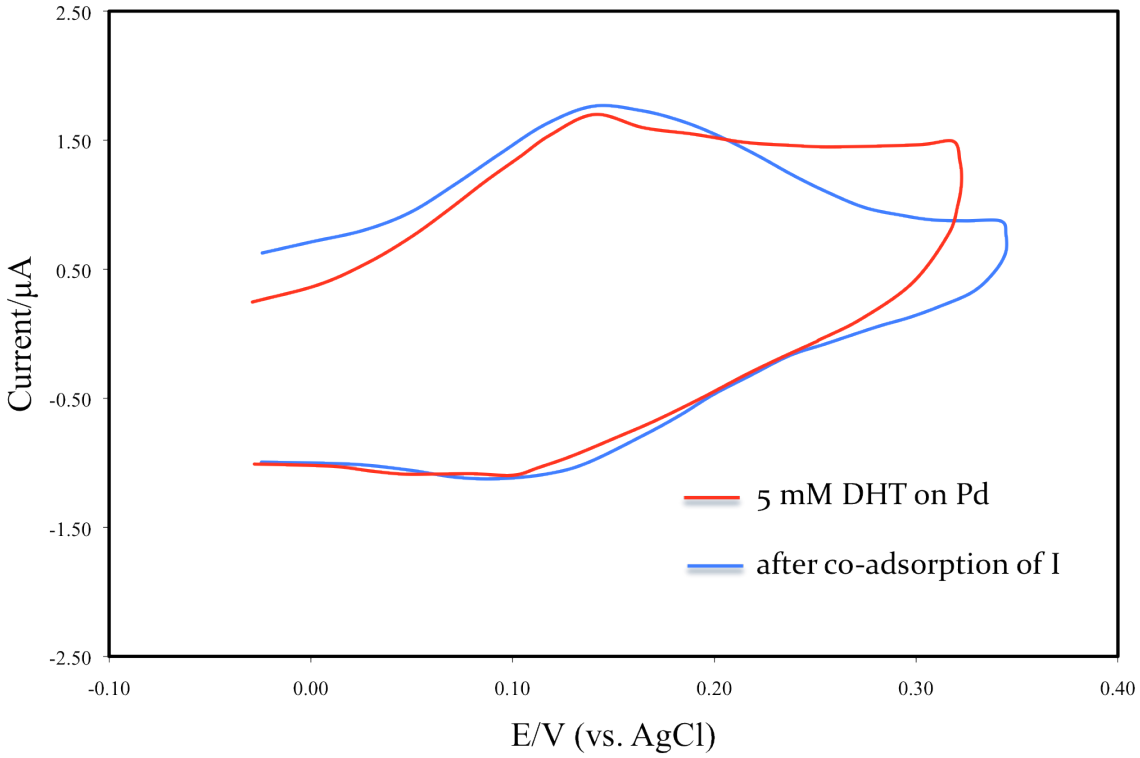

Figure 40. Cyclic voltammograms of chemisorbed DHT on Pd(111) surface prepared from 5 mM solution before (red) and after (blue) coadsorption of I.

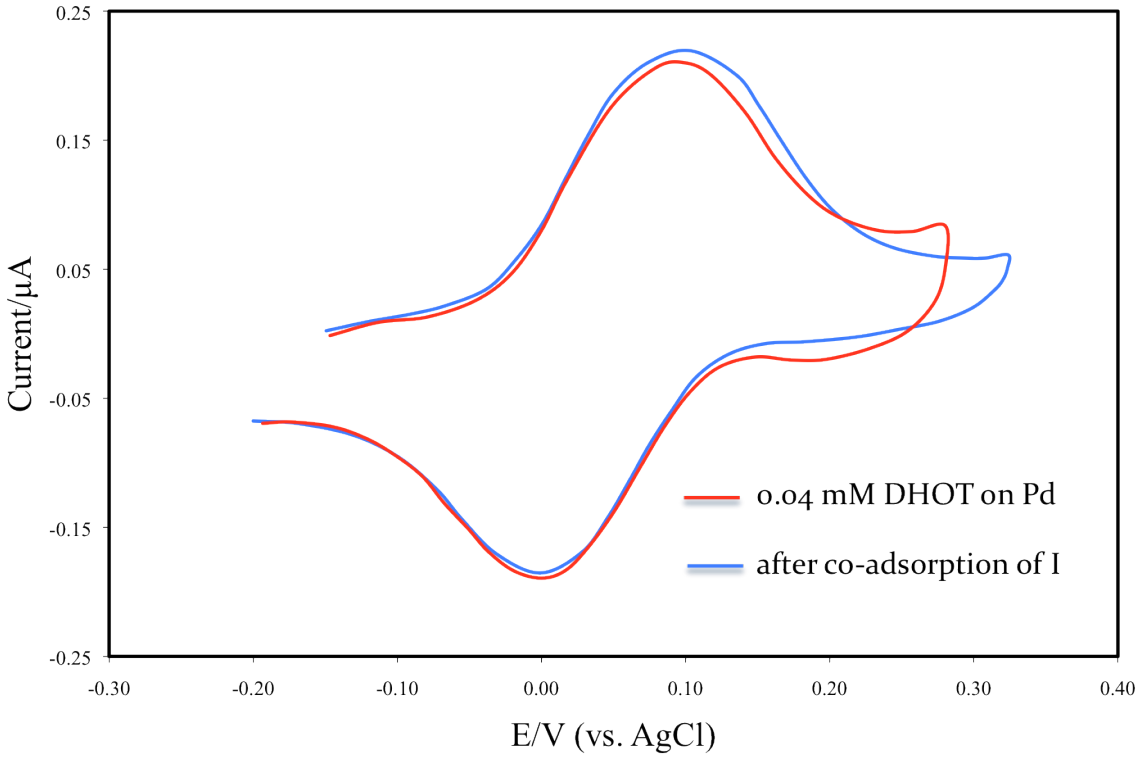

Figure 41. Cyclic voltammograms of chemisorbed DHOT on Pd(111) surface prepared from 0.04 mM solution before (red) and after (blue) co-adsorption of I.

Table 2. HREELS Peak assignments for DHT chemisorbed on Pd(111)

Energy Loss Pd-S-η^7-H_2Q (cm^{-1})	**Energy Loss Pd-S-η^1-H_2Q (cm^{-1})**	**Energy Loss Pt-S-η^1-H_2Q [a] (cm^{-1})**	**Mode[b] Pd-S-η^1-H_2Q**
442	420	409	δ(CC)
803	818	821	γ(CH)
1186	1149,1238	1171	ν(CO) δ(CH)
1437	1407	1463	δ(OH)
1599	1584	1574	ν(CC)
3036	3043	3048	ν(CH)
noisy	noisy	3508	ν(OH)

[a] See Reference[80]

[b] γ ≡ out-of-plane bending, δ ≡ in-plane bending, and ν ≡ stretching

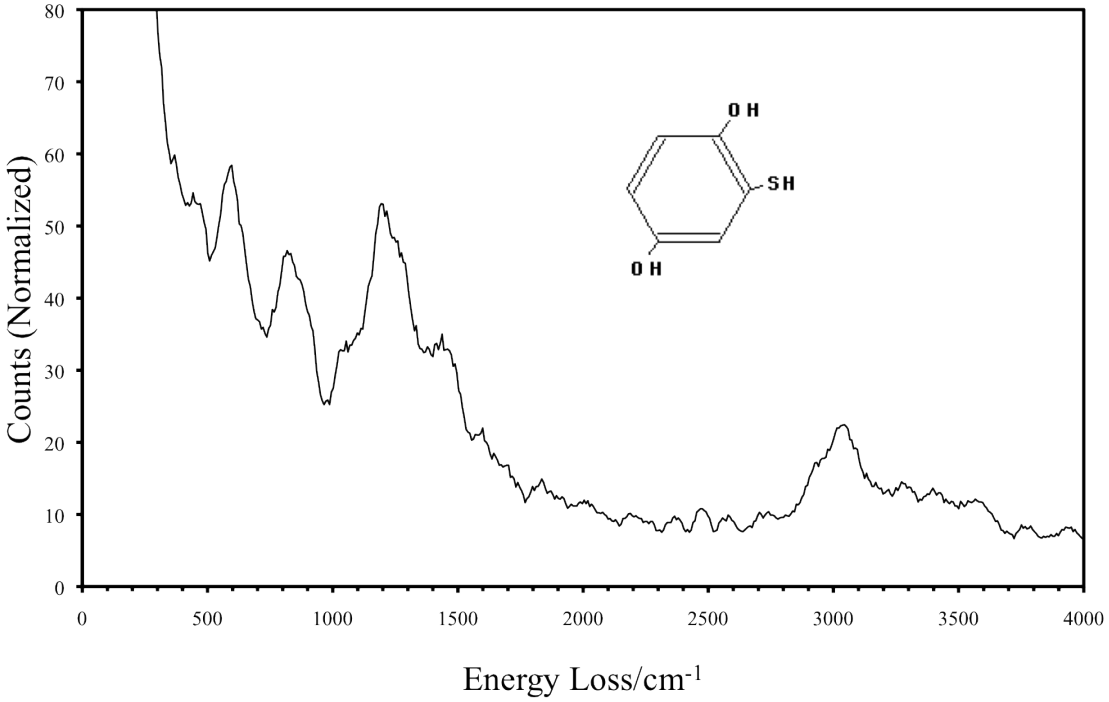

Figure 42. HREEL spectrum of DHT chemisorbed on Pd(111) surface from 0.02 mM solution.

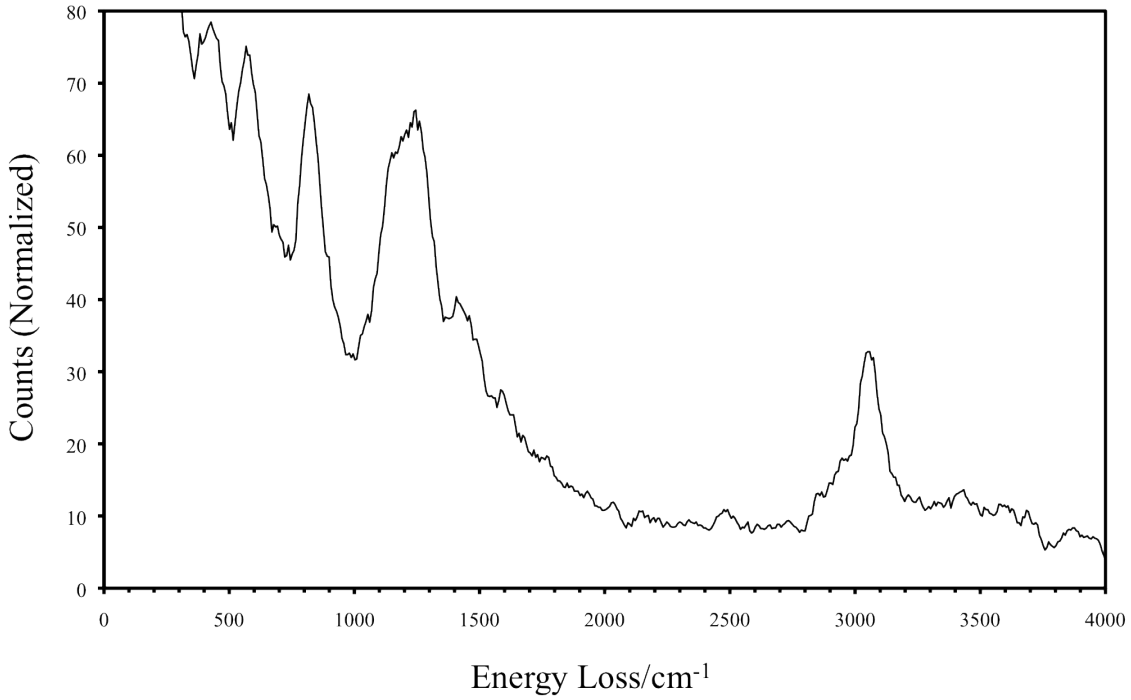

Figure 43. HREEL spectrum of DHT chemisorbed on Pd(111) surface from 5 mM solution.

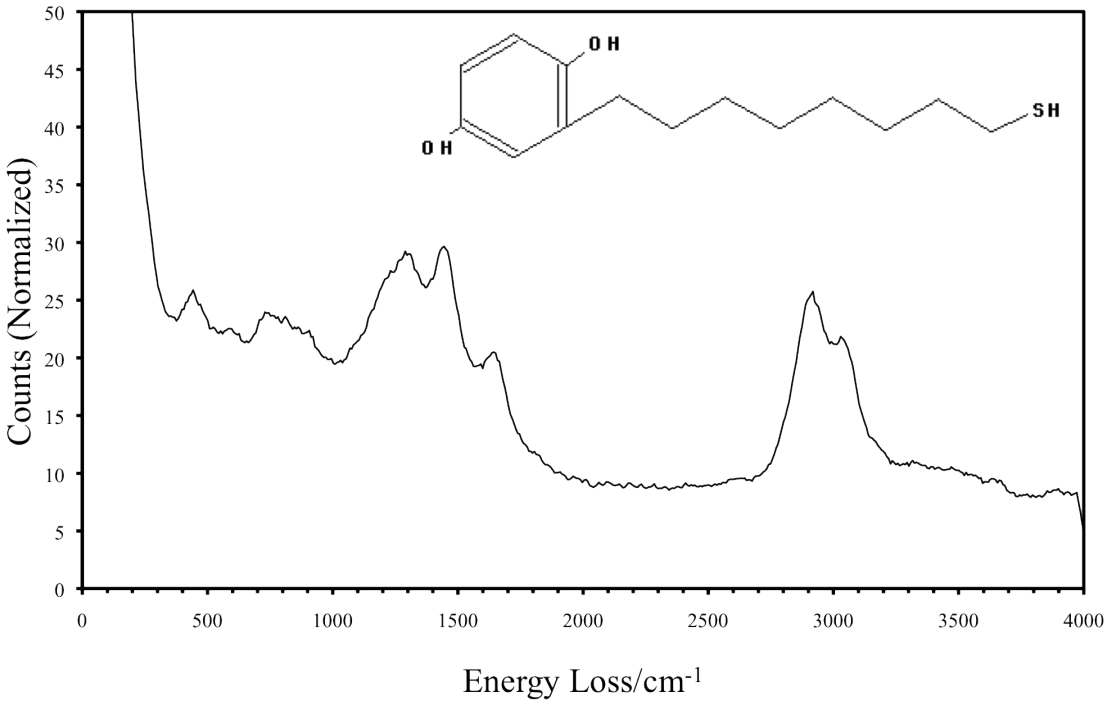

Figure 44. HREEL spectrum of chemisorbed DHOT on Pd(111) surface prepared from 0.04 mM solution.

CHAPTER IV

TRENDS AND CONCLUSIONS

The present work was aimed at an investigation, based on surface-sensitive electron spectroscopy and electrochemistry of the effect of selected functional groups on the chemisorption of aromatic molecules on well-defined Pd(111) single crystal electrode surfaces. The results from this research led to the following trends and conclusions

The results of this work led to the following trends and conclusions: (a) At low concentrations, 2,5-dihydroxythiophenol (DHT) chemisorbs on a Pd surface through both diphenolic ring and thiol group. At high concentrations, it chemisorbs only through the thiol group. (b) There is extensive intermolecular attraction between the co-adsorbed thiolated quinone and thiolated hydroquinone molecules. The interaction occurs through the Pd substrate and not through space. (c) The chemisorption properties of N-heteroaromatic compounds are pH-dependent. When the nitrogen heteroatom is protonated, it becomes very weakly surface-active. When the nitrogen heteroatom is deprotonated, surface activity stronger than the diphenolic ring is exhibited. (d) On a palladium surface, the binding strengths of ligands increase in the order: phenyl ring < quinonoid ring, < N-heteroatom < I < -SH.

REFERENCES

(1) Somorjai, G. A. *Introduction to Surface Chemistry and Catalysis*; John Wiley & Sons: New York, 1994.

(2) Lide, D. R. *Handbook of Chemistry and Physics.*; CRC: Boca Raton, FL, 1998.

(3) Sridharan, V. *Annu. Rep. Prog. Chem. B* **1999**, *95*, 97.

(4) Sterzo, C. L. *Synlett* **1999**, *11*, 1704.

(5) McGlacken, G. P.; Fairlamb, I. J. S. *Eur. J. Org. Chem.* **2009**, *24*, 4011.

(6) Yorimitsu, H.; Oshima, K. *Bull. Chem. Soc. Jpn.* **2009**, *82*, 778.

(7) Gutnov, A.; GmbH, C. *Eur. J. Org. Chem.* **2008**, *27*, 4547.

(8) Kotov, V.; Scarborough, C. C.; Stahl, S. S. *Inorg. Chem. 46*, 1910.

(9) Reiser, O. *Angew. Chem. Int. Ed.* **2006**, *45*, 2838.

(10) Anson, A.; Lafuente, E.; Urriolabeitia, E.; Navarro, R.; Benito, A. M.; Maser, W. K.; Martinez, M. T. *J. Alloys Compd.* **2007**, *436*, 294.

(11) Barsellini, D.; Visintin, A.; Triaca, W. E.; Soriaga, M. P. *J. Power Sources* **2003**, *124*, 309.

(12) Kim, Y.-G.; Soto, J. E.; Chen, X.; Park, Y.-S.; Soriaga, M. P. *J. Electroanal. Chem.* **2003**, *554-555*, 167.

(13) Soto, J. E.; Kim, Y.-G.; Soriaga, M. P. *Electrochem. Commun.* **1999**, *1*, 135.

(14) Kim, Y.-G.; Baricuatro, J. H.; Soriaga, M. P. *Langmuir* **2006**, *22*, 10762.

(15) Chen, X.; Sanabria-Chinchilla, J.; Soriaga, M. P. *Electroanalysis* **2005**, *17*, 2121.

(16) Kim, Y.-G.; Soriaga, M. P. *J. Colloid Interface Sci.* **1999**, *236*, 197.

(17) Waddill, G. D.; Kesmodel, L. L. *Phys. Rev. B: Condens. Matter,* **1985**, *31*, 4940.

(18) Rodriguez, J. F. M., Thomas; Soriaga, Manuel P. *J. Electroanal. Chem.* **1987**, *233*, 283-289.

(19) Chen, X. *Chemisorption and anodic oxidation of aromatic molecules on pd electrode surfaces: Studies by uhv-ec-stm*; Ph.D. Dissertation, Texas A&M University, 2004.

(20) Sanabria-Chinchilla, J. *Electrochemical hydrogenation of aromatic compounds chemisorbed at polycrystalline and single-crystal pd surfaces*; Ph.D. Thesis, Texas A&M University, 2006.

(21) Soriaga, M. P.; Hubbard, A. T. *J. Am. Chem. Soc.* **1982**, *104*, 2735-2742.

(22) Soriaga, M. P.; Hubbard, A. T. *J. Am. Chem. Soc.* **1982**, *104*, 2742.

(23) Pauling, L. C. *Nature of the Chemical Bond*; Cornell University Press: New York, 1960.

(24) Seah, M. P.; Dench, W. A. *Surf. Interface Anal.* **1979**, *1*, 2.

(25) Soriaga, M. P. *Prog. Surf. Sci.* **1992**, *39*.

(26) McCash, E. M. *Surface Chemistry*; Oxford: New York, 2001.

(27) Kolasinski, K. W. *Surface Science: Foundations of Catalysis and Nanoscience*; John Wiley & Sons, New York, 2001.

(28) Ertl, G.; Kuppers, J. *Low Energy Electrons and Surface Chemistry*; VCH: Weinheim, 1985.

(29) Oura, K.; Lifshits, V. G.; Saranin, A. A.; Zotov, A. V.; Katayama, M. *Surface Science: An Introduction*; Springer: Berlin, 2003.

(30) Feldman, L. C.; Mayer, J. W. *Fundamentals of Surface and Thin Film Analysis*; Prentice Hall: Upper Saddle River, NJ, 1986.

(31) Salaita, G. N.; Hubbard, A. T. *Molecular Design of Electrode Surfaces*; Wiley: New York, 1989.

(32) Vickerman, J. C. *Surface Analysis: The Principle Techniques*; John Wiley: Chichester, 1997.

(33) Shoeffel, J. A.; Hubbard, A. T. *Anal. Chem.* **1977**, *49*, 2330.

(34) Hubbard, A. T.; Stickney, J. L.; Rosasco, S. D.; Soriaga, M. P.; Song, D. *J. Electroanal. Chem.* **1983**, *150*, 165.

(35) LK-Tech 2010.

(36) Niemantsverdriet, J. W. *Spectroscopy in Catalysis*; Wiley-VCH: Weinheim, 2000.

(37) Ibach, H.; Mills, D. L. *Electron Energy Loss Spectroscopy and Surface Vibrations*; Academic Press: New York, 1982.

(38) Kesmodel, L. L. *Surface Imaging and Visualization*; CRC Press: Boca Raton, FL, 1995.

(39) Soriaga, M. P.; Chen, X.; Li, D.; Stickney, J. L. In *Applications of Physical Methods to Inorganic and Bioinorganic Chemistry*; Scott, R. A., Lukehart, C. M., Eds.; Wiley: Chichester, UK, 2007, p 171-188.

(40) Thiry , P. A. *Physica Scripta* **1971**, *35*, 229.

(41) Gregorie, C.; Yu, L. M.; Bodino, F.; Tronc, M.; Pireaux, J. J. *J. Electron. Spectrosc. Relat. Phenom.* **1999**, *98-99*, 67.

(42) Lambin, P.; Henrard, L.; Thiry, P.; Silien, C.; Virneron, J. P. *J. Electron. Spectrosc. Relat. Phenom.* **2003**, *129*, 281.

(43) Crescenzi, M. D.; Pianocastelli, M. N. *Electron Scattering and Related Spectroscopies*; World Scientific: Singapore, 1996.

(44) Mills, D. L. *Applied Physics A* **2007**, *87*, 427.

(45) Li, D. *UHV-EC Operation and Maintainance Manual*; Texas A&M University: College Station, 2010.

(46) Yates, J. T.; Madey, T. E. *Vibrational Spectroscopy of Molecules on Surfaces*; Plenum Press: New York, 1987.

(47) Jungwirthova, J.; Kesmodel, L. L. *J. Phys. Chem. B,* **2001**, *105*, 674.

(48) Morin, C.; Simon, D.; Sautet, P. *J. Phys. Chem. B,* **2004**, *108*, 5653-65.

(49) Clark, S. J. S., M. D.; Pickard, C. J.; Hasnip, P. J.; Probert, M. J.; Refson, K.; Payne, M. C. *Z. Kristallogr.* **2005**, *220*, 567.

(50) Qian, H. Q. M., H. Y.; Song, F.; Shi, S. Q.; Zhang, H. J.; Li, H. Y.; He, P. M.; Bao, S. N. *Appl. Surf. Sci.* **2010**, *256*, 2686.

(51) Morin, C. S., D.; Sautet, P. *J. Phys. Chem. B,* **2003**, *107*, 2995.

(52) Perdew, J. P. W., Y. *Phys. Rev. B: Condens. Matter* **1992**, *45*, 13244.

(53) Perdew, J. P. B., K.; Ernzehof, M. *Phys. Rev. Lett.* **1996**, *77*, 386.

(54) Alcalay, W. *Helv. Chim. Acta* **1947**, *30*, 578.

(55) Davis, L. E.; Macdonald, N. C.; Palmberg, P. W.; Riach, G. R.; Weber, R. E. *Handbook of Auger Electron Spectroscopy*; Physical Electronic Industries, Inc.: Eden Prairie, MN, 1976.

(56) Soriaga, M. P. *Chem. Rev.* **1990**, *90*, 771.

(57) Soriaga, M. P.; Mukerjee, S.; Rodriguez, J. A. *Curr. Top. Electrochem.* **1993**, *2*, 45.

(58) Soto, J. E. *Molecular adsorption at well-defined palladium electrode surfaces*; Ph. D. Dissertation. Texas A&M University, 2000.

(59) Hoffman, R. *Solids and Surfaces: A Chemist View of Bonding in Extended Structures*; VCH: New York, 1989.

(60) Hartley, F. R. *The Chemisrtry of Platinum and Palladium*; Wiley: New York, 1973.

(61) Loffreda, D.; Simon, D.; Sautet, P. *Surf. Sci.* **1999**, *425*, 68.

(62) Somorjai, G. A. *Surf. Sci.* **1993**, *280*, 298.

(63) Kim, Y.-G.; Soriaga, M. P. *Physical Chemistry Chemical Physics* **2001**, *3*, 3303.

(64) Schreiber, F. *Surf. Sci.* **2005**, *65*, 151.

(65) Javier, A.; Li, D.; Balbuena, P.; Soriaga, M. P. *J. Phys. Chem. C.* Submitted, **2010**.

(66) Kim, Y.-G.; Soriaga, J.; Vigh, G.; Soriaga, M. P. *J. Colloid Interface Sci.* **2000**, *227*, 505.

(67) Sanabria-Chinchilla, J.; Baricuatro, J. H.; Soriaga, M. P.; Hernandez, F.; Baltruschat, H. *J. Colloid Interface Sci.* **2007**, *314*, 152.

(68) Advanced-Chemistry-Development. V8.14 ed. 1994-2010.

(69) Mebrahtu, T. B., Ginger M.; Bravo, Beatriz G.; Michelhaugh, Susan L.; Soriaga, Manuel P. *Langmuir* **1988**, 1147-51.

(70) Bothwell, M. E.; Rodriguez, J. A.; Soriaga, M. P. *J. Electroanal. Chem.* **1988**, *252*, 453.

(71) Bothwell, M. E.; Soriaga, M. P. *J. Electroanal. Chem.* **1989**, *260*, 193.

(72) Berry, G. M.; Binamira-Soriaga, E.; Soriaga, M. P. *Colloids Surf., A* **1997**, *134*, 31.

(73) Bravo, B. G.; Michelhaugh, S. L.; Soriaga, M. P. *Langmuir* **1989**, *5*, 1092.

(74) Laviron, E. *J. Electroanal. Chem.* **1979**, *100*, 263.

(75) Laviron, E. *J. Electroanal. Chem.* **1979**, *101*, 19.

(76) Kim, Y.-G.; Soriaga, M. P. *J. Colloid Interface Sci.* **2001**, *236*, 197.

(77) Wyckoff, R. W. *Crystal Structure*; Interscience: New York, 1953.

(78) Bravo, B. G.; Michelhaugh, S. L.; Soriaga, M. P. *J. Electroanal. Chem.* **1988**, *241*, 199.

(79) Bravo, B. G.; Mebrahtu, T.; Soriaga, M. P.; Zapien, D. C.; Hubbard, A. T.; Stickney, J. L. *Langmuir* **1987**, *3*, 595.

(80) Roberts, J. T.; Friend, C. M. *J. Chem. Phys.* **1988**, *88*, 7172.

(81) Rei Vilar, M.; Lang, P.; Botelho do Rego, A. M. *Langmuir* **2003**, *19*, 2649.

(82) Kato, H. S.; Noh, J.; Hara, M.; Kawai, M. *J. Phys. Chem. B,* **2002**, *106*, 9655.

VITA

Ding Li

Department of Chemistry
Texas A&M University
College Station, TX, 77843, USA
Work: (979) 845-6914
Home: (979) 422-0969
E-mail: sam.sting@gmail.com

EDUCATION

Ph.D., Chemistry. Texas A&M University, College Station, TX. 2010
B.S., Chemistry. Peking University, Beijing, China. 2000

SELECTED PUBLICATIONS

"Surface Coordination Chemistry Of 2,5-Dihydroxythiophenol At Well-Defined Pd(111) Electrodes: Studies By LEED, AES, HREELS And ElectroChemistry." Soto, J. E.;Li, D.; Sanabria-Chinchilla, J.; Chen, X.; Soriaga, M. P. *J. Molecular Structure*, **2008**, 890(1-3), 298.

"High Resolution Electron Energy Loss Spectroscopy" in *Encyclopedia of Inorganic Chemistry*. Soriaga, M. P.; Chen, X.; Li, D. John Wiley & Sons, New York, **2008**.

"Molecular Chemisorption At Electrocatalyst Surfaces." Kar, P.; Cummins, K.; Baricuatro, J.; Hossain, M.; Li, D.; Soriaga, M. P. *ECS Transactions*, **2007**, 3 (34) 187.

SELECTED PRESENTATIONS

235th National Meeting of American Chemical Society, New Orleans, LA, **2008**, Poster: "Electrocatalyzed oxidation and hydrogenation of hydroquinone on well-defined Pd(hkl)", Li, D; Chen, X.; Sanabria-Chinchilla, J.; Kim Y. G.; Soriaga, M. P.

62nd Southwest Regional Meeting of the American Chemical Society. Houston, TX, **2006**, Poster: "Electrocatalyzed oxidation and hydrogenation of hydroquinone on well-defined Pd(100)", Li, D.; Chen, X.; Sanabria-Chinchilla, J.; Soriaga, M. P.